
Electronic Thesis and Dissertation Repository

8-13-2015 12:00 AM

Investigation of Endogenous In-Vivo Sodium Concentration in Human Prostate Cancer Measured With ^{23}Na Magnetic Resonance Imaging

Justin C. Peterson
The University of Western Ontario

Supervisor
Timothy Scholl
The University of Western Ontario

Graduate Program in Medical Biophysics

A thesis submitted in partial fulfillment of the requirements for the degree in Master of Science

© Justin C. Peterson 2015

Follow this and additional works at: <https://ir.lib.uwo.ca/etd>



Part of the [Medical Biophysics Commons](#)

Recommended Citation

Peterson, Justin C., "Investigation of Endogenous In-Vivo Sodium Concentration in Human Prostate Cancer Measured With ^{23}Na Magnetic Resonance Imaging" (2015). *Electronic Thesis and Dissertation Repository*. 3039.

<https://ir.lib.uwo.ca/etd/3039>

This Dissertation/Thesis is brought to you for free and open access by Scholarship@Western. It has been accepted for inclusion in Electronic Thesis and Dissertation Repository by an authorized administrator of Scholarship@Western. For more information, please contact wlsadmin@uwo.ca.

INVESTIGATION OF ENDOGENOUS *IN-VIVO* SODIUM CONCENTRATION IN
HUMAN PROSTATE CANCER MEASURED WITH ^{23}Na MAGNETIC
RESONANCE IMAGING

(Thesis format: Integrated)

by

Justin Charles Peterson

Faculty of Medicine & Dentistry
Graduate Program in Medical Biophysics

A thesis submitted in partial fulfilment
Of the requirements for the degree of
Master of Science

The School of Graduate and Postdoctoral Studies
The University of Western Ontario
London, Ontario, Canada

© Justin Charles Peterson 2015

Abstract

Prostate cancer (PCa) is the most common malignancy in men. Aggressive prostate tumours must be identified, differentiated from indolent tumours, and treated to ensure survival of the patient. Currently, clinicians use a combination of multi-parametric magnetic resonance imaging (mpMRI) contrasts to improve PCa detection. While these techniques provide very good spatial resolution, the specificity is often insufficient to unequivocally identify malignant lesions.

Utilizing specialized MRI hardware developed for sensitive *in-vivo* detection of sodium, this work has investigated differences in sodium concentration between healthy and malignant prostate tissue. Patients with biopsy-proven PCa underwent conventional mpMRI and sodium MRI followed by radical prostatectomy. Subsequent whole-mount histopathology of the excised prostate was then contoured according to Gleason Grade, a radiological assessment of tumour stage and aggressiveness for PCa. Tissue sodium concentration (TSC) measured by sodium MRI was successfully co-registered with standard image contrasts from multi-parametric MRI and also with pathologist confirmed histopathology as the gold standard.

This proposed method provides quantitative, *in-vivo* sodium information from cancerous human prostates. The results of this study establish the relationship between TSC and malignant PCa, which could prove useful in initial characterization of the disease and for active surveillance of indolent lesions.

Keywords

Sodium (^{23}Na), Prostate Cancer, Magnetic Resonance Imaging (MRI), Tissue Sodium Concentration (TSC)

Acknowledgements

I would like to acknowledge my sincere gratitude to my supervisors Drs. Robert Bartha and Timothy Scholl for their guidance, support, encouragement, and overall patience. I am grateful for the new opportunities and experiences gained while working with these mentors. Their direction, professional support, and assistance, have provided me with an invaluable education.

I would like to thank the third member of my advisory committee, Dr. Aaron Ward for his time, suggestions and helpful advice.

To my colleague Adam Farag, without his knowledge, technical help and dedication, this project would not have happened. To members of my lab, Dr. Francisco Martinez, Yonathan Araya and Heesung (Patrick) Lim, I am grateful and owe many thanks for all their help and involvement in my project. Thank you for the insightful discussions and assistance with the RF development, MR imaging protocols, data processing and the overall project.

I would like to acknowledge the members of the 2nd floor Imaging Research Laboratories for their help throughout my masters including Trevor Szekeres, David Reese, and Dr. Trevor Wade.

I would also like to acknowledge everyone involved in the IGPC-2 Trial, without whom, my project would not have happened including Dr. Glenn Bauman, Dr. Joseph Chin, Dr. Stephen Pautler, Dr. Catherine Hildebrand, Dr. Cesare Romagnoli, Ashley Lozanski, Cathie Crukley, and Dr. Mena Gaed.

I would like to thank Dr. Eli Gibson for his image registration software and Peter Martin for their assistance and troubleshooting skills with said software.

I wish to thank all my family for their love and words of encouragement that led me down this path to where I am today. Finally, I would like to thank Kathryn for her treasured support, motivation and love throughout my graduate career.

Table of Contents

Abstract.....	ii
Acknowledgements.....	iii
Table of Contents.....	v
List of Figures.....	vii
List of Tables.....	vii
List of Abbreviations.....	viii
Chapter 1 (Introduction).....	1
1.1 The Prostate Gland.....	1
1.2 Prostate Cancer.....	2
1.2.1 Statistics.....	2
1.2.2 Symptoms.....	2
1.2.3 Screening.....	3
1.2.4 Grading & Staging.....	4
1.2.5 Cell Metabolism & Regulation.....	8
1.3 Basics of MRI.....	10
1.4 Sodium MRI.....	14
1.4.1 Basics of Sodium MRI.....	14
1.4.2 Bi-Exponential Decay of Sodium.....	14
1.4.3 Separating Signal Components.....	15
1.4.4 Disease Applications.....	16
1.5 References.....	18
Chapter 2 (Methods).....	25
2.1 RF Hardware.....	25
2.2 Imaging Phantoms.....	28
2.3 Specific Absorption Rate Measurements.....	29
2.4 Image Processing.....	29
2.9 References.....	31
Chapter 3 (Manuscript For Submission to Radiology).....	32
3.1 Introduction.....	32
3.2 Methods.....	35
3.2.1 Patients.....	35
3.2.2 Sodium Imaging Exam Protocols.....	37
3.2.3 <i>Ex-Vivo</i> Imaging Exam.....	37
3.2.4 Whole-Mount Histopathology.....	38
3.2.5 Registration.....	38
3.2.6 Statistical Analysis.....	40

3.3 Results	41
3.4 Discussion & Conclusion	44
3.5 References	49
Chapter 4 (Discussion & Future Work).....	54
4.1 Discussion	54
4.1.1 Overview	54
4.1.2 Clarification	54
4.1.3 Clinical Significance	55
4.2 Future Work	56
4.2.1 Twisted Projection Imaging	56
4.2.2 RF Hardware Improvements	57
4.2.3 Additional MRI Contrast Comparisons	58
4.3 Conclusion	58
4.4 References	60
Appendix A – Supplementary Methods.....	62
Appendix B – Hardware Approval	65
Appendix C – Human Participant Approval	69
Appendix D – Data Collection Form	70
Appendix E – Curriculum Vitae	79

List of Figures

Figure 1: Anatomy of the prostate gland. The peripheral zone (purple), central zone (red), transition zone (blue), and the anterior fibromuscular stroma (green), as well as the urethra (yellow) are shown.

Figure 2: Gleason Grades 1-5, where Gleason Grade 1 are least aggressive and Gleason Grade 5 are most aggressive. With increasing Gleason Grade, prostate gland structures are decreasingly differentiated. As Gleason Grade progresses, gland patterns shift from well defined units to fused or poorly defined units with no internal lumina.

Figure 3: a) shows the transmit only asymmetrical birdcage coil b) shows the Mark-3 endorectal (ER) surface coil used to receive the sodium signal. Both resonators were tuned to the Larmor frequency of sodium at 3 Tesla.

Figure 4: The registration pipeline for all imaging data involved in the study. The ^{23}Na volume, a) and body coil *in-vivo* T_2 -weighted volume, b) are registered to the endorectal *in-vivo* T_2 -weighted volume, c). The contoured histopathology, d) and the *ex-vivo* T_1 - and T_2 -weighted volumes (panels e) and f), respectively) are also registered to the endorectal *in-vivo* T_2 -weighted volume.

Figure 5: A representative, unregistered, coloured map of the tissue sodium concentration (TSC) in one slice with its corresponding measurement uncertainty in percentage. Central and transitional zones are combined, with the peripheral zone outlined separately.

Figure 6: Three patients with biopsy proven prostate cancer underwent ^{23}Na MRI to determine the TSC in different grades of tumour tissue. Each patient shows a strong correlation between Gleason Grade and TSC, with a significant difference between lower (Gleason 3+4) and higher (Gleason 4+3) lesions.

Figure 7: (a) high-resolution T_2 -weighted ^1H Cube image, (b) an axially acquired ^1H T_2 -weighted image, (c) and the distribution of endogenous sodium concentration (d-f) with corresponding histology contours overlaid of an oblique slice through a prostate with biopsy-proven cancer. Grey contours represent prostatic intraepithelial neoplasia (PIN, a possible precursor to cancer); green contours represent Gleason 3, Gleason 3+4, and Gleason 4+3 lesions.

List of Tables

Table 1: Clinically relevant information for three patients who completed the study, including pre-treatment procedures, screening bloodwork, and post radical prostatectomy procedures.

List of Abbreviations

$[\text{Na}^+]_{\text{ex}}$	Extracellular Sodium Concentration
$[\text{Na}^+]_{\text{in}}$	Intracellular Sodium Concentration
^{23}Na	Sodium
ADC	Apparent Diffusion Coefficient
AFS	Anterior Fibromuscular Zone
AJCC	American Joint Committee on Cancer
ATP	Adenosine Triphosphate
B_0	Main Magnetic Field
bbefgre3D	3D Efficient Fast Gradient-Recalled Echo
CZ	Central Zone
DCE	Dynamic Contrast-Enhanced
DRE	Digital Rectal Exam
DWI	Diffusion-Weighted Imaging
ER	Endorectal
EVF	Extracellular Volume Fraction
FID-CSI	Free Induction Decay – Chemical Shift Imaging
FOV	Field of view
GRE	Gradient-Recalled Echo
H&E	Hematoxylin and Eosin
HEC	Hydroxyethyl Cellulose
IGPC-2	Image Guided Prostate Cancer-2
IVF	Intracellular Volume Fraction

M_0	Net Magnetization
mpMRI	Multi-Parametric Magnetic Resonance Imaging
MR	Magnetic Resonance
MRI	Magnetic Resonance Imaging
NCCN	National Comprehensive Cancer Network
NEX	Number of Excitations
NHE1	Na^+/H^+ Exchanger
PCa	Prostate Cancer
PCPT	Prostate Cancer Prevention Trial
PIN	Prostatic Intraepithelial Neoplasia
PSA	Prostate Specific Antigen
PZ	Peripheral Zone
QALE	Quality-Adjusted Life Expectancy
RF	Radio Frequency
ROI	Region of Interest
SAR	Specific Absorption Rate
SNR	Signal-to-Noise Ratio
T	Tesla
T_1	Longitudinal Relaxation Time
T_1 -w	T_1 -weighted
T_2	Transverse Relaxation Time
T_2 -w	T_2 -weighted
TNM	Tumour, Node, and Metastasis

TPI	Twisted Projection Imaging
TPS	Thin-Plate Spline
TR	Repetition Rate
TSC	Tissue Sodium Concentration
TZ	Transitional Zone
UTE	Ultra-short Echo Time
γ	Gyromagnetic Ratio
ω_0	Larmor Frequency

Chapter 1

1 Introduction

1.1 The Prostate Gland

The prostate is a walnut-sized organ whose primary function is to produce fluids (prostatic fluid) associated with male reproduction. Prostatic fluid makes up 30% of semen, by volume, with the remaining 70% made up of spermatozoa and seminal vesicle fluid (1). The prostate is located directly below the urinary bladder and surrounds the location where the prostatic urethra and the ejaculatory ducts merge. A small amount of smooth muscle contained within the prostate aids with ejaculation, a secondary function for the prostate (2).

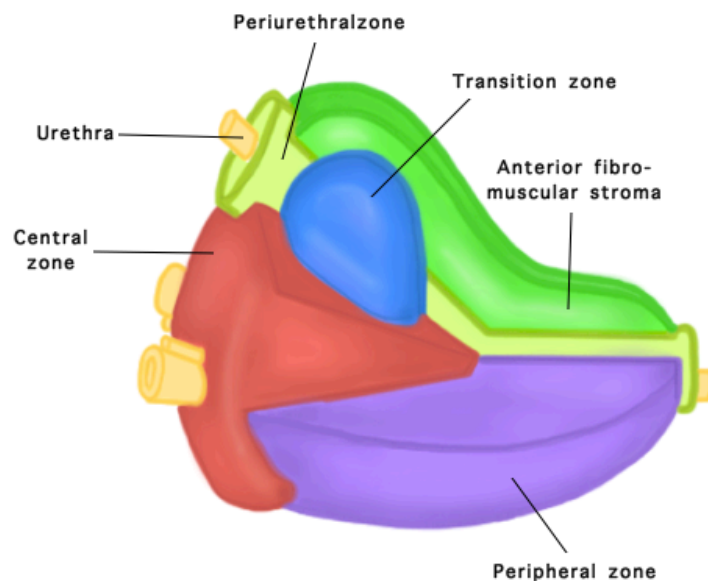


Figure 1; Anatomy of the prostate gland. The peripheral zone (purple), central zone (red), transition zone (blue), and the anterior fibromuscular stroma (green), as well as the urethra (yellow) are shown.

Four zones define the prostate gland (**Figure 1**): central, transitional, anterior fibromuscular, and peripheral. The central zone (CZ) surrounds the ejaculatory ducts and makes up roughly 20% of the prostate by volume. The transitional zone (TZ) surrounds the proximal urethra and comprises 5% of prostatic volume. The peripheral zone (PZ) comprises 70% of the prostate by volume and surrounds the CZ, TZ as well as the distal urethra. Finally, the anterior fibromuscular zone (AFS) comprises 5% of the prostate and is comprised of only fibrous and smooth muscle elements (3).

1.2 Prostate Cancer

1.2.1 Statistics

Prostate Cancer (PCa) is the most common malignancy for men in Canada, with one in eight diagnosed overall. In 2014, there were 23,600 new cases of PCa in Canada alone with 40% of men diagnosed between the ages of 60-69. Men who are diagnosed with PCa have a relatively low probability (1 in 28) of death but also experience a diminished quality of life (4). Most cases of PCa (99%) are adenocarcinoma, which is defined as neoplasia of epithelial tissue with glandular origin, glandular characteristics, or both (5). Between 2001 and 2009, the mortality rate of PCa declined significantly, this is most likely due to improved treatment options and/or the introduction of the prostate-specific antigen (PSA) test but studies reported conflicting results (6,7).

1.2.2 Symptoms

Though early forms of PCa do not present symptoms, advanced stage symptoms range from: prostatic bleeding, blood present in semen, bone pain, and urinary obstruction. Patients could misinterpret lower urinary tract disease as urinary obstruction, which occurs due to benign prostatic enlargement.

1.2.3 Screening

According to the National Comprehensive Cancer Network (NCCN) practice guidelines, asymptomatic PCa suspicions begin with an abnormal digital rectal exam (DRE). In this process, a physician will palpate the prostate through the rectum to determine any irregularities. Regardless of the outcome of other metrics, symptomatic patients receive a bone scan to test for metastases. The NCCN also recommends the use of the PSA test, which as many studies have concluded, is a controversial method (8).

Centres that use the PSA test as a risk evaluation tool (among other metrics) set a threshold at which the patient should undergo biopsy. The level of antigen present in the blood stream in order for a patient to undergo biopsy varies. While there is a correlation between increasing risk of PCa and increasing PSA levels, there is no lower limit, which eliminates the risk altogether (9). PSA thresholds set at 3 and 4 ng/ml had false positives rates of 19.8% and 11.3%, respectively (10,11). The Prostate Cancer Prevention Trial (PCPT) studied nearly 19,000 men between October 1993 and June 2003 in the United States (12). The trial reported findings of PCa for 15% of men with a PSA < 4 ng/ml and normal DRE, 30-35% of men with 4 ng/ml < PSA < 10 ng/ml, and 67% of men with a PSA > 10 ng/ml (13,14).

Patients with positive PSA test results are scheduled for further screening techniques, including prostate biopsy. Prostate biopsy is a procedure in which twelve core samples of prostate tissue are systematically acquired by needle biopsy from the rectum. This procedure is often aided by image-guided techniques such as ultrasound or magnetic resonance imaging (MRI). Possible side effects of prostate biopsy include hematuria (blood present in urine), infection, hospital admission, and in some cases death. An

observational study of 1000 men who underwent prostate biopsy noted that patients had experienced side effects such as: hematuria (31%), infection (0.9%), hospitalization (2.1%), and death (0.2%) (15).

Overdiagnosis is a term used when disease is correctly detected but would not cause noticeable symptoms or death and is an inevitable consequence of screening for disease. The prevalence of overdiagnosis in PCa varies according to the frequency of screening, threshold of the PSA test used, patient age, number of core samples taken, and disease risk (16). It has been shown that 40-56% of men screened who received a diagnosis of PCa can be attributed to overdiagnosis (15). While there has been a reduction in PCa mortality from 38% in 1995 to 22% in 2006, quality of life has become a relevant concern related to the problem of benefit versus harm.

1.2.4 Grading & Staging

Gleason Grading

Donald F. Gleason established the gold standard grading system for PCa in 1966. Appropriately named the Gleason system; it has been amended twice in 1974 and 1977 by Gleason himself (17). The system is based upon low-power, microscopic observation of morphological features of prostate tissue classified by Gleason. All tumours are judged to fit within 5 categories, representing different states of complexity in morphology. A tumour is graded depending on the most prevalent (primary) and the second most prevalent (secondary) observed Gleason Grade. The combination of these two gradings is called a Gleason Score (primary grade + secondary grade = Gleason Score) (18). Many reports have confirmed the significance of Gleason Scoring and outcome after no treatment (19), treatment with radical prostatectomy (20), and radiation therapy (21).

Prostatic Intraepithelial Neoplasia (PIN) describes a lesion that, although isn't cancerous, could be a possible precursor to malignancy (9). PIN is most easily described as the presence of prominent nuclei within an existing duct structure. The similarities between PIN and prostatic carcinoma include: increased severity and incidence with age and prominence within the PZ of the prostate (22). Benign Prostatic Hyperplasia (BPH) is the formation of benign nodules within the prostate due to an increase in cell proliferation. In some cases these nodules can obstruct the urethra, leading to painful urination (8).

A Gleason Grade of 1 (**Figure 2(1)**) describes tissue that is uniform, comprised of separate, closely packed glands. Gleason Grades 1 and 2 are very well-differentiated and in most cases today would be considered atypical adenomatous hyperplasia by immunohistochemistry (18). Grades 1 and 2 patterns diagnosed from needle core biopsies were given a higher grade at radical prostatectomy, and also had poor reproducibility; therefore they are rarely assigned (23).

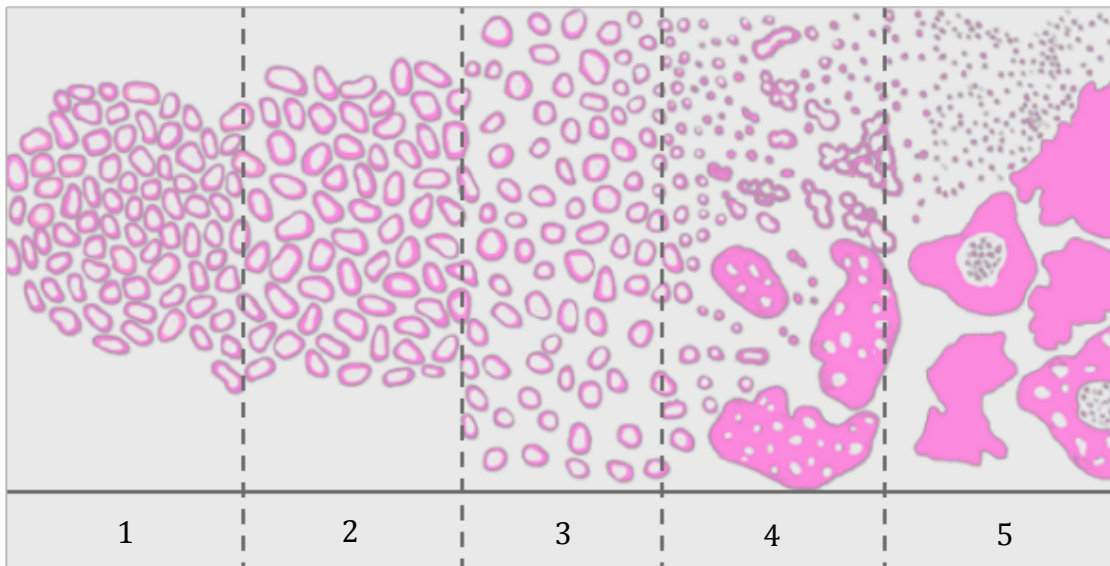


Figure 2; Gleason Grades 1-5, where Gleason Grade 1 are least aggressive and Gleason Grade 5 are most aggressive. With increasing Gleason Grade, prostate gland structures are decreasingly differentiated. As Gleason Grade progresses, gland patterns shift from well defined units to fused or poorly defined units with no internal lumina.

Gleason Grade from biopsy is reliable and significant for Gleason Grade 3, which represents the most common Gleason patterns reported from biopsy. In Grade 3, gland units are typically smaller than Gleason patterns 1 and 2; infiltration between benign glands is common (**Figure 2(3)**). In Gleason 3, gland units are still distinguishable with a defined border, a distinction that separates Gleason 3 from Gleason 4.

In Gleason 4, a new tissue characteristic is introduced. Cribriform structures are described as large irregular glands without recognizable lumina. Gleason 4 could also present as fused, ill-defined glands with poorly formed glandular lumina (**Figure 2(4)**). One consideration pathologists need to beware of is tangential sectioning, where the biopsy needle's trajectory is such that it bisects the glands at an angle that distorts the appearance of the gland units. Tangential sectioning creates the impression of ill-defined glands with inconspicuous lumina that could lead to a false-positive diagnosis as Gleason 4 (24).

The most aggressive pattern in the Gleason grading system is Gleason 5, where there is no longer any glandular differentiation (**Figure 2(5)**). In pattern 5, the cribriform structures from Gleason 4 are upgraded with central comedonecrosis. Comedonecrosis is the presence of necrotic cells within the luminal space of the gland and/or karyorrhexis, where the nucleus of a dying cell is distributed irregularly throughout the cytoplasm (24,25).

The distinction between Gleason Grade 3 and 4 is an extremely important one. This is a threshold that the NCCN (9) and Cancer Care Ontario (CCO) (26) has set to determine which patients will undergo active surveillance (these patients will have routine follow-

up examinations at set time intervals) and those patients who require immediate treatment (these patients will undergo treatment procedures such as radical prostatectomy, brachytherapy, and chemotherapy). By correctly distinguishing patients into therapy groups, patients can be spared psychological and physical pain from unnecessary treatment; as well as save an estimated \$100 million in healthcare costs per annum in Canada alone (27).

Staging

In order to deliver a clear diagnosis; clinicians use a staging system to distil all prognostic factors into a single classification. The most commonly used staging system for prostate cancer is the American Joint Committee on Cancer (AJCC) tumour, node, and metastasis (TNM) system. Further subcategories of each classification are used to describe the cancer in detail (8).

To describe the size and invasion of the tumour, “T classification” is used.

- T1: the tumour is not apparent by DRE nor visible by imaging
- T2: the tumour is confined to the prostate gland
- T3: the tumour extends beyond the prostatic capsule
- T4: the tumour is fixed or invades adjacent structures

To describe lymph node metastasis, “N classification” is used.

- NX: lymph nodes were not assessed
- N0: no regional lymph node metastasis
- N1: metastasis present in regional lymph nodes

Finally, if the cancer has spread past the lymph nodes, “M classification” is used.

- M0: no distant metastasis
- M1: distant metastasis

1.2.5 Cell Metabolism & Regulation

The regulation of intracellular pH is important for cellular function; it plays a role in cell proliferation, invasiveness, drug resistance and apoptosis (28–30). Proliferative cancer cells in solid tumours increase anaerobic glycolysis to compensate for hypoxia due to the limited diffusion of oxygen across tissue (31,32). This increased anaerobic glycolysis leads to a reduction of tumour pH through increased lactate production and hypoxic adenosine triphosphate (ATP) hydrolysis. As a mechanism to prevent apoptosis, the cell will increase proton efflux, regulating intracellular pH (33). One of the systems used by cells to regulate pH is the Na^+/H^+ (NHE1) antiport, which is inherently coupled to the transport of Na^+ ions across cellular membranes (34–36). This antiport facilitates the exchange of extracellular Na^+ for intracellular H^+ . It has been shown that the NHE1 exchanger could also play a role in initiation of cell growth and proliferation (37,38). A study by Rotin *et al.* demonstrated that human tumour cells lacking the NHE1 exchanger either lost or severely reduced their ability to grow tumours (30). An upregulation of the NHE1 antiporters is a mechanism used to cope with intracellular acidification, which in turn increases intracellular sodium concentration (30,36,39,40). Expression of the NHE1 antiport has been observed to affect tumour cell migration through extracellular acidification (41). Tumour cells metastasize through the metastatic cascade, in which the cell migration step is dependent upon the degradation of the extracellular matrix through acid extrusion (42). Based on solid tumours, increased intracellular sodium levels would likely be expected as an inherent result of upregulated NHE1 (32). Cameron *et al.* showed that “...rapidly dividing cells had significantly higher sodium concentration than did the slowly dividing cells but significantly less sodium than did the tumor cells” (28). Intracellular sodium concentration ($[\text{Na}^+]_{\text{in}}$) is largely regulated by a combination of

NHE1 (influx) and Na^+/K^+ ATPase (efflux) and can vary by large amounts. Extracellular sodium concentration ($[\text{Na}^+]_{\text{ex}}$) rarely deviates from plasma concentrations, which is regulated by renal sodium exchange and tissue perfusion (28,39,40,43). Tissue Sodium Concentration (TSC) is a weighted average of the $[\text{Na}^+]_{\text{in}}$ and $[\text{Na}^+]_{\text{ex}}$ based on relative intracellular volume (IVF) and extracellular volume fractions (EVF). $[\text{Na}^+]_{\text{ex}}$ is essentially kept constant at ~ 140 mmol/L with sufficient tissue perfusion (44), while normal $[\text{Na}^+]_{\text{in}}$ is ~ 10 - 15 mmol/L (45–47). A study by Langer *et al.* showed that EVF decreased from 68.8% to 52.1% while IVF increased in PCa when compared to normal prostate tissue (48). Assuming a constant $[\text{Na}^+]_{\text{ex}}$, an IVF of 46.2% and an EVF of 52.1%, $[\text{Na}^+]_{\text{in}}$ can be calculated for a given TSC value. Intracellular sodium concentration is an indirect measure of cell malignancy and mobility (28,41). Therefore a non-invasive method capable of quantifying tissue sodium concentration could prove useful in assessing cancerous tissue.

1.3 Basics of MRI

Magnetic Resonance Imaging (MRI) is a diagnostic modality that is unrivalled in its ability to produce excellent soft-tissue contrast images of biological systems high spatial resolution and with no ionizing radiation (49). Developed in the early 1970s, the number of clinical MRI units has grown to an estimated 25,000 with 266 systems installed in Canada (50). To produce contrast, MRI exploits the interaction of nuclear spins within an applied magnetic field. The most common nuclide utilized is the proton of the water molecule because of its high abundance in the body (80 mol/L), intrinsic nuclear spin of $\frac{1}{2}$ and large magnetic dipole moment. A fundamental physical property of nuclei, nuclear spin is a combination of contributions from both unpaired protons and neutrons. Not all nuclei are observable by MRI; only those that possess a non-zero-spin value. When placed in a magnetic field, the magnetic dipole moments of non-zero-spin nuclei precess around the magnetic field direction and will preferentially align, to a small degree, with the magnetic axis. In the case of MRI, this axis exists along the bore of the magnet and, by convention, is denoted by the letter z in a Cartesian axis system. This creates a small net magnetization (M_0) along the magnetic field direction. However, in the absence of a dominant magnetic field, the angles of the precession of spins with respect to the z -axis are randomly distributed resulting in no net magnetization. A particular nuclide precesses at a specific frequency within a uniform magnetic field, termed the Larmor frequency (ω_0). The Larmor frequency of a nuclide is proportional to the strength of the field in which it is placed (B_0) and is given by

$$\omega_0 = 2\pi\gamma B_0 \quad (1.3.1)$$

where γ , the proportionality constant, is called the nuclear gyromagnetic ratio measured in Hertz per Tesla. The gyromagnetic ratio is unique for each nuclide. Clinical MR systems vary in magnetic field strength, measured in Tesla (T), from low-field (0.2T) to high field (7T) systems. Most MRI scanners in operation today utilize a field strength of 1.5T but in recent years there has been a large increase in the number of higher field strength magnets (3-7T) (50). Higher field strengths have the advantage of an increased signal to noise ratio (SNR) for MRI associated with greater magnetization and higher Larmor frequencies. This can allow for shorter imaging times at higher spatial resolution but comes at the price of higher equipment costs, greater sensitivity to field inhomogeneities, potential tissue heating and electromagnetic coupling between transmit and receive structures (51).

An MRI produces signal by perturbing the bulk magnetization of tissue with radio frequency (RF) waves at the Larmor precessional frequency of protons. As the excited magnetization relaxes back to equilibrium, it emits RF energy, which is also at the Larmor frequency. The RF power is often applied by a dedicated transmit coil. This is a tuned RF circuit, which is resonant at the Larmor frequency of the nuclide of interest. To detect the relaxation of the magnetization, a separate proximal RF receive coil, resonant at the same Larmor frequency can also be used for increased local signal sensitivity. Excitation of the tissue magnetization is accomplished by short pulses of RF power applied to the transmit coil. Before an RF pulse is applied the bulk magnetization is oriented longitudinally aligned along the z -axis. A 90° RF pulse will flip the longitudinal magnetization into the transverse (x - y plane) reducing the longitudinal magnetization to essentially zero. The magnetization then relaxes back to the longitudinal equilibrium state

through different mechanisms. Spin-spin (T_2) and spin-lattice (T_1) are the two predominant relaxation features that affect the excited magnetization immediately following an RF excitation pulse.

Spin-lattice relaxation represents the loss of energy from the spin system to the surrounding lattice (environment). This exchange of energy is a result of local fluctuations in the magnetic field due to interactions of tumbling molecules. Protons in water molecules are tumbling in the environment of these fluctuating magnetic fields and can gain or lose internal energy as a result of these electromagnetic fluctuations they experience. For example, a larger number of magnetic fluctuations at or near the Larmor frequency produce more effective spin-lattice relaxation. This exchange of energy governs how quickly the tissue re-magnetizes after application of an RF excitation pulse and how quickly repeated RF pulses can be applied. The longitudinal magnetization, $M_z(t)$, asymptotically relaxes back to the thermal equilibrium value as $M_z(t) = M_0(1 - e^{-t/T_1})$, where the exponential time constant, T_1 , is the spin-lattice relaxation time governing this process.

Spin-spin relaxation is due to the dephasing of the ensemble of spins from their coherent precession after RF excitation to a nearly uniform distribution in the transverse plane. This dephasing occurs due to slight differences in precessional frequencies for individual spins arising from intrinsic magnetic field inhomogeneities. Apparent magnetic field inhomogeneities experienced by nuclei in molecules are linked to the molecular size and mobility of the molecules. Small, fast tumbling molecules, such as free water effectively average out the magnetic field inhomogeneities, resulting in an apparently relatively homogeneous local field, so that very little dephasing of the spins and longer T_2 (spin-

spin relaxation) times are observed. Nuclei in large, slow tumbling molecules such as fat experience a relatively static magnetic field inhomogeneity, leading to more dephasing of the transverse magnetization and faster signal decay (shorter T_2 times) (49). The receive RF coil detects an oscillating signal at the Larmor frequency with an exponentially decaying amplitude whose exponential time constant is T_2^* , the effective spin-spin relaxation time. T_2^* characterizes the apparent relaxation time due to the inherent sources of magnetic field inhomogeneity mentioned above as well as external sources of inhomogeneity due to imperfect magnetic field shimming and magnetic susceptibility effects related to air/tissue interfaces and iron-containing blood. T_2^* is always shorter than T_2 .

T_1 and T_2 relaxation times are fundamental properties associated with a particular nuclide for a given tissue and are observable as a bulk property. Knowledge of these relaxation times are important for optimizing the imaging parameters of a pulse sequence to garner the most signal from a particular sample or to optimize the image contrast between healthy and cancerous tissue.

1.4 Sodium MRI

1.4.1 Basics of Sodium MRI

As mentioned above, any nuclide that possess a non-zero spin value can, in principle, be detected using MRI. Of particular interest are sodium (^{23}Na) nuclei, which possess a $\frac{3}{2}$ spin value. ^{23}Na MRI is technically difficult because of low sodium concentration in the body (~ 90 mmol/L) versus the concentration of protons (80 mol/L), its low gyromagnetic ratio (1/4 that of protons), and its $\frac{3}{2}$ spin. Sodium MRI is often referred to as ^{23}Na MRI and despite its lack of success during early research (52), it has become more feasible in recent years due to advancements in high-field MRI hardware, pulse sequence software, and widespread implementation of multi-nuclear MRI systems (53–56).

1.4.2 Bi-Exponential Decay of Sodium

^{23}Na MRI is technically difficult due to the limited endogenous sodium concentration and rapid spin-spin relaxation times; however, the very short T_1 relaxation time supports shorter repetition rates (TR), leading to faster signal acquisition and reduced imaging times. Even with TR set to three times the T_1 of ^{23}Na (to allow for quantification of TSC without T_1 corrections), ten RF excitations are possible in one second. In addition to low endogenous concentration, ^{23}Na MRI is challenging due to the intrinsic $\frac{3}{2}$ spin value of sodium nuclei. This higher spin value, compared with that of the proton, results in bi-exponential T_2 relaxation (two distinct components to the exponential signal decay) for sodium (“long component”: 20-30ms and “fast component”: 1-2ms). Sodium nuclei can have four distinct energy levels (Zeeman energies) in a magnetic field, $-\frac{3}{2}$, $-\frac{1}{2}$, $\frac{1}{2}$, and $\frac{3}{2}$ and can transition between each of them. A change between adjacent energy levels is called a

single quantum transition, but changes between other levels are possible, double or triple quantum transitions. Normally in an unrestricted watery solution containing sodium, all transitions are single quantum, and have the same energy. In tissue, the movement of sodium is more restricted - particularly within cells. This alters the relative amount of short versus long component T_2 decay, which is observed. For sodium imaging of tissue, the long and short components comprise approximately 60% and 40% of the signal, respectively. For quantification of TSC, a short acquisition delay (TE) is required to observe both the short and long component T_2 decay, which helps to reduce T_2 losses (52).

1.4.3 Separating Signal Components

Distinguishing between intracellular sodium and extracellular sodium is essential to the success of ^{23}Na MRI in biomedical research. Intracellular sodium reflects the stability of the cellular membrane, as well as the state of cellular metabolism (57), while extracellular sodium is usually fixed by perfusion. The triple quantum filtered (TQF) technique has shown promise as an effective method of separating the signal from these two compartments (58–60). TQF attempts to suppress the extracellular component of the signal through manipulation of the bi-exponential decay due to the quantum transitions between energy states. The TQF approach assumes that the long and short T_2 components of the signal are specific to the extracellular and intracellular compartments, respectively. The experimental difficulty with TQF lies in the low SNR, which leads to longer scan times and reduced resolution. There have also been reports of unwanted extracellular sodium significantly contributing to TQF signals (58,61), therefore caution with this technique is warranted. Bi-exponential weighted ^{23}Na imaging is a promising technique

that utilizes both spin-density weighted and single-quantum-filtered imaging. It offers compartment separation without the drawbacks of low SNR and longer scan times as in TQF (62). The method uses a single-quantum-filtered image, which contains mainly signal from mono-exponentially decaying sodium nuclei and a spin-density weighted image, which contains signal from all sodium ions. The single-quantum-filtered image is subtracted from the spin-density image to produce contrast mainly from the intracellular compartment.

To obtain absolute sodium concentration information, calibration phantoms must be employed. A large volume phantom of concentration 100-150 mmol/L is needed to assess the RF coils, as well as two or more reference phantoms ranging in concentration from 20-150 mmol/L. The reference phantoms were integrated into the RF receive coil. These phantoms both allow absolute sodium concentration measurements as well as provide fiducial markers for registration purposes.

1.4.4 Disease Applications

Sodium MRI can detect changes in metabolism of tissue as well as cellular membrane integrity. Healthy cells maintain a constant ^{23}Na gradient across the cellular membrane. A disruption of the cell membrane or impaired energy metabolism will result in an increase of $[\text{Na}^+]_{\text{in}}$ (57). Significant ^{23}Na changes can be seen in myocardial infarction (63), stroke (44), and cancer (64,65).

Sodium levels have been shown to increase after stroke induced in rats as determined by flame spectrometry of punch samples (66); these findings have since been confirmed with ^{23}Na MRI (67,68). Sodium MRI has also been shown as a possible tool to monitor therapy that causes cell death such as chemotherapy. A xenograft animal model of PCa (69) as well as breast cancer patients undergoing chemotherapy (70) reported a significant decrease in TSC with a decrease in lesion size.

Imaging cancer with ^{23}Na MRI has been a growing area of research due to the fluctuations of $[\text{}^{23}\text{Na}]_{\text{in}}$ in cells with increased mobility and proliferation (30,36–40). Sodium MRI studies have reported an increase in TSC of 50% in both brain and breast cancers compared to normal tissue (64,65), and a doubling of TSC in low-grade glioma (71). ^{23}Na MRI has been employed to measure sodium in the healthy human prostate (72–74) and the cancerous mouse prostate (75) but TSC values have yet to be measured in a cancerous human prostate. The purpose of this thesis is to examine the potential for the use of ^{23}Na MRI in the clinic as a non-invasive tool to aid clinicians in PCa treatment stratification.

1.5 References

1. Huggins, C Scott, WW Heinen J. Chemical composition of human semen and of the secretions of the prostate and seminal vesicles. *Am. J. Physiol.* 1941;136:467–473.
2. Coutsoukis P. *Gray's Anatomy: The Prostate.* 2007.
3. McNeal JE. Normal and pathologic anatomy of prostate. *Urology* [Internet] 1981;17:11–16.
4. Canada S. Canadian Cancer Statistics Special topic : Skin cancers. *Can. Cancer Soc.* 2014;2014:1–132.
5. Anon. Canadian Cancer Society. 2015.
6. Andriole GL, Crawford ED, Grubb RL, et al. Mortality results from a randomized prostate-cancer screening trial. *N. Engl. J. Med.* 2009;360:1310–1319. doi: 10.1056/NEJMoa0810696.
7. Schröder FH, Hugosson J, Roobol MJ, et al. Screening and prostate-cancer mortality in a randomized European study. *N. Engl. J. Med.* 2009;360:1320–1328. doi: 10.1056/NEJMoa0810084.
8. National Comprehensive Cancer Network. NCCN Clinical Practice Guidelines in Oncology (NCCN Guideline®). Prostate cancer. Version 2.2014. 2014.
9. National Comprehensive Cancer Network. NCCN Clinical Practice Guidelines in Oncology (NCCN Guideline®). Prostate Cancer. Early Detection. Version 1.2014. 2014.
10. Croswell JM, Kramer BS, Kreimer AR, et al. Cumulative incidence of false-positive results in repeated, multimodal cancer screening. *Ann. Fam. Med.* 2009;7:212–222. doi: 10.1370/afm.942.
11. Kilpeläinen TP, Tammela TLJ, Roobol M, Hugosson J, Ciatto S, Nelen V, Moss S, Määttänen L, Auvinen A. False-positive screening results in the European randomized study of screening for prostate cancer. *Eur. J. Cancer* 2011;47:2698–2705. doi: 10.1016/j.ejca.2011.06.055.
12. Thompson IM, Goodman PJ, Tangen CM, Parnes HL, Minasian LM, Godley P a, Lucia MS, Ford LG. Long-term survival of participants in the prostate cancer prevention trial. *N. Engl. J. Med.* [Internet] 2013;369:603–10. doi: 10.1056/NEJMoa1215932.

13. Catalona WJ, Smith DS, Ratliff TL, Dodds KM, Coplen DE, Yuan JJJ, Petros JA, Andriole GL. Measurement of Prostate-Specific Antigen in Serum as a Screening Test for Prostate Cancer. *N. Engl. J. Med.* [Internet] 1991;324:1156–1161. doi: 10.1056/NEJM199104253241702.
14. Thompson IM, Pauler DK, Goodman PJ, et al. Prevalence of Prostate Cancer among Men with a Prostate-Specific Antigen Level ≤ 4.0 ng per Milliliter. *N. Engl. J. Med.* [Internet] 2004;350:2239–2246. doi: 10.1056/NEJMoa031918.
15. Dunfield L, Usman A, Fitzpatrick-Lewis D, Shane A. Screening for prostate cancer with prostate specific antigen and treatment of early-stage or screen-detected prostate cancer: a systematic review of the clinical benefits and harms. 2014.
16. Bell N, Gorber SC, Shane A, Joffres M, Singh H, Dickinson J, Shaw E, Dunfield L, Tonelli M, Care CTF on PH. Recommendations on screening for prostate cancer with the prostate-specific antigen test. *Can. Med. Assoc. J.* [Internet] 2014;186:1225–1234. doi: 10.1503/cmaj.140703.
17. Gleason DF. Histologic grading of prostate cancer: A perspective. *Hum. Pathol.* 1992;23:273–279. doi: 10.1016/0046-8177(92)90108-F.
18. Shah RB. Current perspectives on Gleason grading of prostate cancer. *Curr. Urol. Rep.* 2011. doi: 10.1007/s11934-011-0181-5.
19. Schwartz E, Albertsen P. Nomograms for clinically localized disease. Part III: watchful waiting. In: *Seminars in urologic oncology*. Vol. 20. ; 2002. pp. 140–145.
20. Roehl K a, Han M, Ramos CG, Antenor JA V, Catalona WJ. Cancer progression and survival rates following anatomical radical retropubic prostatectomy in 3,478 consecutive patients: long-term results. *J. Urol.* 2004;172:910–914. doi: 10.1097/01.ju.0000134888.22332.bb.
21. Zagars GK, Pollack A, Von Eschenbach AC. Prognostic factors for clinically localized prostate carcinoma: Analysis of 938 patients irradiated in the prostate specific antigen era. *Cancer* 1997;79:1370–1380. doi: 10.1002/(SICI)1097-0142(19970401)79:7<1370::AID-CNCR15>3.0.CO;2-X.
22. Brawer MK. Prostatic Intraepithelial Neoplasia: An Overview. *Rev. Urol.* [Internet] 2005;7:S11–S18.
23. Epstein JI. Gleason score 2-4 adenocarcinoma of the prostate on needle biopsy: a diagnosis that should not be made. *Am. J. Surg. Pathol.* 2000;24:477–478. doi: 10.1097/00000478-200004000-00001.
24. Baydar DE, Epstein JI. Gleason grading system, modifications and additions to the original scheme. *Turkish J. Pathol.* 2009;25:59. doi: 10.5146/tjpath.2009.00975.

25. Zamzami N, Kroemer G. Condensed matter in cell death. *Nature* 1999;401:127–128. doi: 10.1038/43591.
26. Morash C, Tey R, Agbassi C, Klotz L, MCGowan T, Srigley J, Evans A. A Quality Initiative of the Program in Evidence-Based Care (PEBC), Cancer Care Ontario (CCO) Active Surveillance for the Management of Localized Prostate Cancer. 2014.
27. Dragomir A, Cury FL, Aprikian AG. Active surveillance for low-risk prostate cancer compared with immediate treatment : a Canadian cost comparison. 2014;2:60–68. doi: 10.9778/cmajo.20130037.
28. Cameron I, Smith N, Pool T, Sparks R. Intracellular Concentration of Sodium and Other Elements as Related to Mitogenesis and Oncogenesis in Vivo. *Cancer Res.* [Internet] 1980:1493–1500.
29. Nagy I, Lustyik G, Lukács G, Nagy V, Balázs G. Correlation of malignancy with the intracellular Na⁺: K⁺ ratio in human thyroid tumors. *Cancer Res.* [Internet] 1983:5395–5402.
30. Rotin D, Steele-Norwood D, Grinstein S, Tannock I. Requirement of the Na⁺/H⁺ exchanger for tumor growth. *Cancer Res.* [Internet] 1989;49:205–11.
31. Tannock IF. Oxygen diffusion and the distribution of cellular radiosensitivity in tumours. *Br. J. Radiol.* [Internet] 1972;45:515–524. doi: 10.1259/0007-1285-45-535-515.
32. Tannock IF, Rotin D. Acid pH in tumors and its potential for therapeutic exploitation. *Cancer Res.* 1989;49:4373–4384.
33. Roos A, Boron WF. Intracellular pH. *Physiol. Rev.* [Internet] 1981;61:296–434.
34. Călinescu O, Paulino C, Kühlbrandt W, Fendler K. Keeping It Simple, Transport Mechanism and pH Regulation in Na⁺/H⁺ Exchangers. *J. Biol. Chem.* [Internet] 2014;289:13168–76. doi: 10.1074/jbc.M113.542993.
35. He P, Yun CC. Mechanisms of the regulation of the intestinal Na⁺/H⁺ exchanger NHE3. *J. Biomed. Biotechnol.* 2010;2010:238080. doi: 10.1155/2010/238080.
36. Mager T, Rimon A, Padan E, Fendler K. Transport mechanism and pH regulation of the Na⁺/H⁺ antiporter NhaA from *Escherichia coli*: An electrophysiological study. *J. Biol. Chem.* 2011;286:23570–23581. doi: 10.1074/jbc.M111.230235.
37. Grinstein S, Rothstein A. Mechanisms of Regulation of the Na⁺/H⁺ Exchanger. *J. Membr. Biol.* 1986;90:1–12. doi: 10.1007/BF01871271.

38. Moolenaar WH. Effects of growth factors on intracellular pH regulation. *Annu. Rev. Physiol.* 1986;48:363–376. doi: 10.1146/annurev.ph.48.030186.002051.
39. Reshkin SJ, Bellizzi a, Caldeira S, Albarani V, Malanchi I, Poignee M, Alunni-Fabbroni M, Casavola V, Tommasino M. Na⁺/H⁺ exchanger-dependent intracellular alkalinization is an early event in malignant transformation and plays an essential role in the development of subsequent transformation-associated phenotypes. *FASEB J.* 2000;14:2185–2197. doi: 10.1096/fj.00-0029com.
40. Demaurex N, Grinstein S. Na⁺/H⁺ antiport: modulation by ATP and role in cell volume regulation. *J. Exp. Biol.* [Internet] 1994;196:389–404.
41. Stock C, Schwab A. Protons make tumor cells move like clockwork. *Pflugers Arch. Eur. J. Physiol.* 2009;458:981–992. doi: 10.1007/s00424-009-0677-8.
42. Gatenby R a., Gawlinski ET, Gmitro AF, Kaylor B, Gillies RJ. Acid-mediated tumor invasion: A multidisciplinary study. *Cancer Res.* 2006;66:5216–5223. doi: 10.1158/0008-5472.CAN-05-4193.
43. Kometiani P, Liu L, Askari A. Digitalis-Induced Signaling by Na⁺/K⁺ ATPase in Human Breast Cancer Cells. *Mol. Pharmacol.* [Internet] 2005;67:929–936. doi: 10.1124/mol.104.007302.of.
44. Thulborn KR, Gindin TS, Davis D, Erb P. Comprehensive MR imaging protocol for stroke management: tissue sodium concentration as a measure of tissue viability in nonhuman primate studies and in clinical studies. *Radiology* 1999;213:156–166.
45. Keenan MJ, Niedergerke R. Intracellular sodium concentration and resting sodium fluxes of the frog heart ventricle. *J. Physiol.* 1967;188:235–260.
46. Rose CR, Ransom BR. Regulation of intracellular sodium in cultured rat hippocampal neurones. *J. Physiol.* 1997;499 (Pt 3:573–587.
47. Rose CR, Ransom BR. Gap junctions equalize intracellular Na⁺ concentration in astrocytes. *Glia* [Internet] 1997;20:299–307. doi: 10.1002/(SICI)1098-1136(199708)20:4<299::AID-GLIA3>3.0.CO;2-1.
48. Langer DL, van der Kwast TH, Evans AJ, Plotkin A, Trachtenberg J, Wilson BC, Haider M a. Prostate tissue composition and MR measurements: investigating the relationships between ADC, T2, K(trans), v(e), and corresponding histologic features. *Radiology* 2010;255:485–494. doi: 10.1148/radiol.10091343.
49. McRobbie DW, Moore EA, Graves MJ, Prince MR. MRI: From Picture to Proton. 2nd ed.; 2006. doi: 10.1097/00004032-200310000-00020.

50. Rinck PA. *Magnetic Resonance in Medicine. The Basic Textbook of the European Magnetic Resonance Forum.* 8th ed.; 2015.
51. Duyn JH. The future of ultra-high field MRI and fMRI for study of the human brain. *Neuroimage* 2012;62:1241–1248. doi: 10.1016/j.neuroimage.2011.10.065.
52. Ouwerkerk R. *Magnetic Resonance Neuroimaging* Modo M, Bulte JWM, editors. 2011;711. doi: 10.1007/978-1-61737-992-5.
53. Stobbe R, Beaulieu C. Advantage of sampling density weighted apodization over postacquisition filtering apodization for sodium MRI of the human brain. *Magn. Reson. Med.* 2008;60:981–986. doi: 10.1002/mrm.21738.
54. Nielles-Vallespin S, Weber MA, Bock M, Bongers A, Speier P, Combs SE, Wöhrle J, Lehmann-Horn F, Essig M, Schad LR. 3D radial projection technique with ultrashort echo times for sodium MRI: Clinical applications in human brain and skeletal muscle. *Magn. Reson. Med.* 2007;57:74–81. doi: 10.1002/mrm.21104.
55. Clayton DB, Lenkinski RE. MR Imaging of Sodium in the Human Brain with a Sequence at 4 T 1. *Magn. Reson. Med.* 2003;23:4–7.
56. Atkinson IC, Renteria L, Burd H, Pliskin NH, Thulborn KR. Safety of human MRI at static fields above the FDA 8T guideline: Sodium imaging at 9.4T does not affect vital signs or cognitive ability. *J. Magn. Reson. Imaging* 2007;26:1222–1227. doi: 10.1002/jmri.21150.
57. Murphy E, Eisner D a. Regulation of Intracellular and Mitochondrial Sodium in Health and Disease. *Circ. Res.* 2009;104:292–303. doi: 10.1161/CIRCRESAHA.108.189050.
58. Knubovets T, Shinar H, Navon G. Quantification of the contribution of extracellular sodium to ²³Na multiple-quantum-filtered NMR spectra of suspensions of human red blood cells. *J. Magn. Reson.* 1998;131:92–96. doi: 10.1006/jmre.1997.1337.
59. Winter PM, Poptani H, Bansal N. Patrick M. Winter, Harish Poptani, and Navin Bansal 2. 2007;2:2002–2007.
60. Dizon JM, Tauskela JS, Wise D, Burkhoff D, Cannon PJ, Katz J. Evaluation of triple-quantum-filtered ²³Na NMR in monitoring of Intracellular Na content in the perfused rat heart: comparison of intra- and extracellular transverse relaxation and spectral amplitudes. *Magn. Reson. Med.* 1996;35:336–345.
61. Jelicks LA, Gupta RK. On the extracellular contribution to multiple quantum filtered ²³Na NMR of perfused rat heart. *Magn. Reson. Med.* [Internet] 1993;29:130–133. doi: 10.1002/mrm.1910290124.

62. Benkhedah N, Bachert P, Semmler W, Nagel AM. Three-dimensional biexponential weighted ^{23}Na imaging of the human brain with higher SNR and shorter acquisition time. *Magn. Reson. Med.* 2013;70:754–765. doi: 10.1002/mrm.24516.
63. Ouwerkerk R, Bottomley PA, Solaiyappan M, Spooner AE, Tomaselli GF, Wu KC, Weiss RG. Tissue sodium concentration in myocardial infarction in humans: a quantitative ^{23}Na MR imaging study. *Radiology* 2008;248:88–96. doi: 10.1148/radiol.2481071027.
64. Ouwerkerk R, Jacobs M a, Macura KJ, Wolff AC, Stearns V, Mezban SD, Khouri NF, Bluemke D a, Bottomley P a. Elevated tissue sodium concentration in malignant breast lesions detected with non-invasive ^{23}Na MRI. *Breast Cancer Res. Treat.* [Internet] 2007;106:151–60. doi: 10.1007/s10549-006-9485-4.
65. Ouwerkerk R, Bleich K, Gillen J. Tissue Sodium Concentration in Human Brain Tumors as Measured with ^{23}Na MR Imaging. *Radiology* [Internet] 2003;23:529–537.
66. Wang Y, Hu W, Perez-Trepichio a D, Ng TC, Furlan a J, Majors a W, Jones SC. Brain tissue sodium is a ticking clock telling time after arterial occlusion in rat focal cerebral ischemia. *Stroke.* 2000;31:1386–1391; discussion 1392. doi: 10.1161/01.STR.31.6.1386.
67. Jones SC, Kharlamov A, Yanovski B, Kim DK, Easley K a., Yushmanov VE, Ziolk SK, Boada FE. Stroke onset time using sodium MRI in rat focal cerebral ischemia. *Stroke* 2006;37:883–888. doi: 10.1161/01.STR.0000198845.79254.0f.
68. Yushmanov VE, Yanovski B, Kharlamov A, Laverde G, Boada FE, Jones SC. Sodium mapping in focal cerebral ischemia in the rat by quantitative ^{23}Na MRI. *J. Magn. Reson. Imaging* 2009;29:962–966. doi: 10.1002/jmri.21643.
69. Kline RP, Wu EX, Petrylak DP, Szabolcs M, Alderson PO, Weisfeldt ML, Cannon P, Katz J. Rapid in Vivo Monitoring of Chemotherapeutic Response Using Weighted Sodium Magnetic Resonance Imaging. 2000;6:2146–2156.
70. Jacobs MA, Ouwerkerk R. Multinuclear and Multiparametric MR Imaging as an early treatment response biomarker for preoperative systemic therapy in breast cancer: Preliminary Results. In: Vol. 006973. ; 2009. p. 103175.
71. Bartha R, Megyesi JF, Watling CJ. Low-grade glioma: Correlation of short echo time ^1H -MR spectroscopy with ^{23}Na MR imaging. *Am. J. Neuroradiol.* 2008;29:464–470. doi: 10.3174/ajnr.A0854.
72. Hausmann D, Konstandin S, Wetterling F, Haneder S, Nagel AM, Dinter DJ, Schonberg SO, Zollner FG, Schad LR. Apparent diffusion coefficient and sodium

concentration measurements in human prostate tissue via hydrogen-1 and sodium-23 magnetic resonance imaging in a clinical setting at 3T. *Invest. Radiol.* [Internet] 2012;47:677–682. doi: 10.1097/RLI.0b013e318267bc6f.

73. Bae KT, Kim J-H, Furlan A, Moon C, Park B, Zhao T. Proton and sodium MR imaging of in vivo human prostate using dual-tuned body and endorectal coils at 7T. In: Vol. 1. ; 2010. p. 5273.

74. Wetterling F, Corteville DM, Kalayciyan R, Rennings A, Konstandin S, Nagel AM, Stark H, Schad LR. Whole body sodium MRI at 3T using an asymmetric birdcage resonator and short echo time sequence: first images of a male volunteer. *Phys Med Biol* 2012;57:4555–4567. doi: 10.1088/0031-9155/57/14/4555.

75. Near J, Bartha R. Quantitative sodium MRI of the mouse prostate. *Magn Reson Med* 2010;63:822–827. doi: 10.1002/mrm.22196.

Chapter 2

2 Hardware Construction and Testing

The contents of this chapter were previously published by Farag *et al.*, for which I was second author (1).

2.1 RF Hardware

To acquire signal from sodium nuclei two pieces of RF hardware were designed and built in the 2nd Floor Imaging RF Engineering Laboratory at the Robarts Research Institute. The first was a birdcage transmit-only coil (designed and built by Adam Farag (1)) with an asymmetric cross section used to excite the sodium nuclei at their specific Larmor frequency (Figure 3a).

To achieve this, the quasi-elliptical cross-section of an MR 750 GE 3T was determined and a volume resonator large enough for a human torso was constructed for RF excitation of the sodium magnetization. The top half of the resonator assembly is detachable from the bottom to facilitate easy patient access. The resonator itself was constructed of 16 copper tubes functioning as rungs held in place by two Delrin® plastic end rings machined to match the elliptical cross sections of the usable bore volume. The asymmetric coil was tuned to resonate at the Larmor frequency of sodium nuclei at 3T (33.78 MHz) according to values calculated in Farag *et al.* (1).

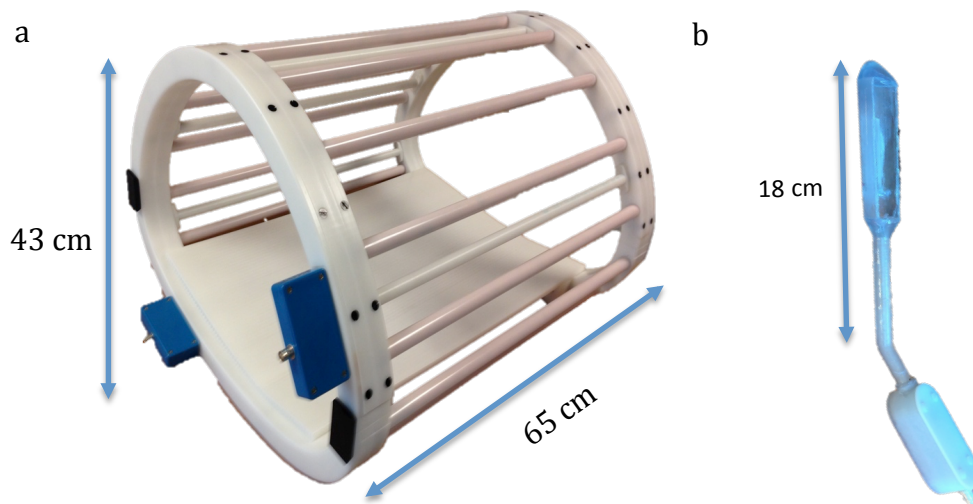


Figure 3: a) The transmit-only asymmetrical birdcage coil. b) The Mark-3 endorectal (ER) surface receive-only sodium coil. Both resonators were tuned to the Larmor frequency of sodium at 3 Tesla (33.78 MHz).

The second piece of RF hardware designed and constructed was a rigid endorectal (ER) surface coil to receive signal from the sodium nuclei at their specific Larmor frequency (constructed by Adam Farag and myself (1)) (Figure 3b). A rigid design was chosen for simplicity and to facilitate co-registration of ^{23}Na MRI and mpMRI imaging data. Multiple versions of the probe were designed and constructed before the final design was chosen. I coated all the probes with biocompatible sealant (MS151 MED, Masterbond, NJ), which acted as a fluid-resistant seal as well as an additional layer of heat and electrical insulation.

The Mark-1a ER probe contained a dual-tuned RF loop for both ^1H (127.74 MHz) and ^{23}Na (33.78 MHz) while the Mark-1b contained only a single tuned RF loop for ^{23}Na imaging. Adam Farag manufactured the identical shells of the Mark-1a/b endorectal coils from polycarbonate using 3D printing. The ER probe consisted of two separate volumes; the proximal section inserted into the subject contained the RF circuit loop, while the stem/base section housed the wires connecting the circuit with the balun and matching circuitry in an adjoined external box. The Mark-1 probes had insufficient internal volume within the proximal end to house reference calibration vials, which are essential for absolute TSC measurement; therefore a larger Mark-2 version was constructed.

The single tuned (^{23}Na -only) Mark-2 endorectal coil was 3D printed by Adam Farag from ABS-M30 by FOCUS® with all essential sections incorporated into one solid piece. The proximal end housed the RF circuit loop as well as three one-millilitre reference calibration vials (which I constructed and implemented) containing 30, 90 and 150 mmol/L concentrations of NaCl in water. The stem section housed the wires connecting the RF loop and the balun and matching circuits, which were contained within the distal end of the probe. When inserted, the rigid, straight-stem design of the Mark-1 and -2 was determined to interfere with the MR bed and affected the anatomy of the patient.

To resolve the interference of the probe and MR bed and improve patient comfort, a third and final single tuned (^{23}Na -only) probe was constructed (Mark-3). While the Mark-3 ER coil contained identical RF circuitry to the Mark-2, the difference between the Mark-2

and -3 was the incorporation of a 45° bend in the stem section and the ability to separate the proximal/stem section from the distal section.

2.2 Imaging Phantoms

To test and calibrate the RF hardware, five phantoms were constructed:

- 1) a prostate-sized saline phantom of diameter 2.9 cm and NaCl concentration of 154 mmol/L, used for SNR and B_1 measurements of the endorectal probes,
- 2) a hollow torso phantom of diameter 34.3 cm, used for loading the asymmetric birdcage for B_1 measurements,
- 3) a large cylindrical saline phantom of diameter 27.4 cm and NaCl concentration 154 mmol/L, used for mapping the B_1 field within the asymmetric birdcage,
- 4) a small cylindrical saline phantom of diameter 15 cm, used for mapping the 3D sensitivity profile of the endorectal probes by submersion,
- 5) a body-tissue-equivalent homogenous phantom, used in specific absorption rate (SAR) measurements of the endorectal probes.

Imaging parameters for all phantoms can be found in Farag *et al.* (1).

2.3 Specific Absorption Rate Measurements

The specific absorption rate (SAR) surrounding the endorectal probes was measured to be within acceptable levels, so not as to increase the temperature of surrounding tissue by more than 1°C (2). This was measured using a body-tissue-equivalent homogenous phantom filled with hydroxyethyl cellulose (HEC) gel with electrical conductivity matching that of human tissue (0.27 S/m). Six individual optically coupled temperature transducers were placed on the probes, while two were inserted into the gel near the probes. The temperature transducers had a precision of 0.1°C and their values were recorded at a frequency of 10 Hz for the duration of the imaging time.

2.4 Image Processing

The raw ^{23}Na data were imported into Matlab (Mathworks, Natick, MA), where a k -space Gaussian filter (34×34 , SD: 9) was applied before Fourier transformation. All ^{23}Na image sets of 10 NEX were registered together using the three reference calibration vials as fiducials. The images were then averaged together to improve SNR; image sets with significant motion during acquisition were discarded. The averaged *in-vivo* volumes were then sensitivity corrected using a saline phantom volume, acquired with the ^{23}Na endorectal coil submersed in the small cylindrical phantom with a diameter of 15 cm. ^{23}Na calibration data collected from this phantom used acquisition parameters identical to those used for the *in-vivo* ^{23}Na data collection. Calibration of the ER RF surface coil's receive profile was carried out using the method described in Axel *et al.* (3). To obtain absolute TSC values from the ^{23}Na data, the known sodium concentrations of the vials

were plotted against average signal intensity values for the regions of interest (ROI) corresponding to the internal calibration vials. The tissue sodium concentration was calculated from

$$TSC = \left(\frac{S_T}{S_{Ph}} \right) / U \quad (2.6.1)$$

where, S_T and S_{Ph} were the signal within a voxel in the tissue and small, cylindrical, saline phantom data, respectively. The quantity, U , is the slope acquired from the plot of signal intensity versus sodium concentration. **Eq 2.6.1** is adapted from Wetterling *et al.* (4). The TSC uncertainty (E_{TSC}) in each voxel was calculated according to **Eq 2.6.2**, where SNR_T and SNR_{Ph} are the SNR in each voxel of the tissue image and phantom image, respectively. The parameter, δU , represents the uncertainty in determination of the slope, U .

$$E_{TSC} = \left[\sqrt{\left(\frac{1}{SNR_T} \right)^2 + \left(\frac{1}{SNR_{Ph}} \right)^2 + \left(\frac{\delta U}{U} \right)^2} \right] * TSC \quad (2.6.2)$$

2.5 References

1. Farag A, Peterson JC, Szekeres T, Bauman G, Chin J, Romagnoli C, Bartha R, Scholl TJ. Unshielded asymmetric transmit-only and endorectal receive-only radiofrequency coil for ^{23}Na MRI of the prostate at 3 tesla. *J. Magn. Reson. Imaging* [Internet] 2014:n/a–n/a. doi: 10.1002/jmri.24798.
2. NEMA. Determination of local specific absorption rate (SAR) in diagnostic magnetic resonance imaging. 2006.
3. Axel L, Costantini J, Listerud J. Intensity Correction in Surface-Coil MR Imaging. *Am. J. Roentgenol.* 1987;148:418–420.
4. Wetterling F, Tabbert M, Junge S, Gallagher L, Macrae IM, Fagan AJ. A double-tuned $(^1\text{H})/(^{23}\text{Na})$ dual resonator system for tissue sodium concentration measurements in the rat brain via Na-MRI. *Phys. Med. Biol.* 2010;55:7681–7695. doi: 10.1088/0031-9155/55/24/019.

Chapter 3

3 Manuscript For Submission to Radiology

Title: *In-Vivo* Sodium MRI of Prostate Cancer: Correlations with Gleason Grade Using Whole Mount Pathology

3.1 Introduction

One in seven men will develop prostate cancer (PCa) in their lifetime and most of these men will die with this disease, rather than as a result of it (1). Since the introduction of the prostate specific antigen (PSA) screening test, there has been a concern regarding overdiagnosis of clinically insignificant disease and therefore over-treatment (2–4). Overdiagnosis has been shown to negatively affect the quality of life of patients as well as being an economic burden on the healthcare systems (5). Diagnosis involves ranking specific PCa lesions according to Gleason Grade, the gold standard scale from one to five that is based on the differentiation of prostate gland units as scored by a pathologist on routine hematoxylin and eosin (H&E) microscopy. The Gleason Score, a combination of the primary and secondary grade present, is inherently related to tumor aggressiveness and the strongest prognostic and predictive factor in the disease and therefore is an essential assessment tool for guiding treatment plans (6–8). Urologists use transrectal ultrasound-guided biopsy cores to estimate Gleason Score for patient-specific treatment planning. Unfortunately, the biopsy only samples approximately 0.2% of the prostate and carries an approximate 30-40% risk of under sampling clinically significant foci of prostate cancer (9–11). The use of an alternative imaging-based method for estimation of

tumor grade would be a significant benefit. Non-invasive identification of potentially high-grade foci in the gland could be used to direct prostate biopsy or guide focal treatment approaches. Early in the treatment pipeline, accurate determination of the Gleason Score is essential to place patients in the proper treatment schemes according to tumor grade (for example, active surveillance for men with low grade, low volume lesions) in order to optimize patient outcomes and the use of health care resources.

Multi-parametric magnetic resonance imaging (MRI) is emerging as a method to improve non-invasive PCa grading (12). Currently, clinicians use a combination of multi-parametric MRI including T_2 -weighted, diffusion-weighted, and dynamic contrast enhanced imaging to improve PCa detection (13,14). ^1H contrast-enhanced imaging exploits vascular volume and cellular organization changes through uptake of a gadolinium contrast agent. While these techniques provide high spatial resolution, the specificity is often insufficient to localize malignant lesions and assign a tumor grade. In addition, current mpMRI interpretation relies on qualitative suspicion scores (PIRADS scale), which are subject to inter-observer variation and require expert reading skills (15). Thus an imaging test that could provide complimentary information about the location and grade of intraprostatic cancer foci would be valuable.

Sodium (^{23}Na) MRI has been shown to reveal important information about biochemical and physiological processes within tissue. The tissue sodium concentration (TSC) in normal tissue is a sensitive indicator of cellular integrity and energy metabolism (16–18). TSC is a weighted average of the intracellular ($[\text{Na}^+]_{\text{in}}$) and extracellular sodium concentrations ($[\text{Na}^+]_{\text{ex}}$), based on relative intracellular volume (IVF) and extracellular volume fractions (EVF). $[\text{Na}^+]_{\text{ex}}$ is essentially kept constant at ~ 140 mmol/L with

sufficient tissue perfusion (19), while normal $[\text{Na}^+]_{\text{in}}$ is $\sim 10\text{-}15$ mmol/L (20–22). Therefore, the mechanisms in which TSC can vary are through extracellular volume changes (cellular organization, density) or through changes in intracellular sodium concentration (altered metabolism) (23,24).

^{23}Na MRI can be employed to obtain information about a combination of both intracellular and extracellular changes within tissue. Increased activity of the sodium-proton (Na^+/H^+) antiport (25,26) and sodium-potassium (Na^+/K^+ -ATPase) pump (17,27) in cells have been linked to tumor malignancy. A study by Cameron *et al.* (1980) concluded that slowly dividing cells had significantly lower $[\text{Na}^+]_{\text{in}}$ than rapidly dividing cells, while tumour cells showed significantly higher $[\text{Na}^+]_{\text{in}}$ than both slow and fast dividing cells (17). Previous studies have shown increased TSC in brain and breast cancer measured by MRI (18,24). While *in-vivo* endogenous sodium imaging has been demonstrated in both mouse (28) and human prostates (29,30), TSC has not been measured in human prostate cancer. We have previously developed a transmit-only receive-only (TORO) combination of an asymmetric birdcage coil and an endorectal coil that provided sufficient sensitivity to image ^{23}Na nuclei in the human prostate (31). The purpose of the current study was to correlate *in-vivo* quantification of sodium with Gleason Score in patients with PCa. In the work presented here, histologically identified prostate cancer was registered to *in-vivo* human sodium imaging data using a previously published and validated registration pipeline (32) that incorporates *in-vivo* ^1H images acquired during the same MR exam as well as *ex-vivo* ^1H images of the prostate obtained after prostatectomy. This study is the first to relate *in-vivo* MRI measured TSC of human prostate cancer with histopathologically confirmed Gleason Score.

3.2 Methods

3.2.1 Patients

Seven male patients (aged 61 ± 5) (**Table 1**) with biopsy-proven prostate cancer were recruited between June 2013 and November 2014 in conjunction with a multi-modality, image-guided prostate cancer study (IGPC-2) (32). In addition to the usual exclusion criteria for MR studies (implanted devices etc.), men were excluded from this study if they had prior therapy for PCa, use of 5-alpha reductase inhibitors (e.g. Finasteride or Dutasteride) within 6 months of the study start, a prostate volume greater than 68 cc (whole mount pathology limit), allergies to contrast agents and other administered agents, insufficient renal function, and a residual bladder volume greater than 150 cc. Patients were instructed to drink 30 mL of milk of magnesia the night before the MR exam and to fast 12 hours prior to the exam.

Category	Patient 1	Patient 2	Patient 3
Age	65	64	53
Pre-Treatment Procedures			
Pre-biopsy PSA (ng/mL)	14.96	5.05	4.22
Primary Pattern	3	3	3
Secondary Pattern	4	4	4
Overall Gleason Score	7	7	7
Prostate Volume (cc)	45	30	25
Clinical T-Stage	cT2c	cT2c	cT1c
Screening Bloodwork			
Creatinine (μmol/L)	76	64	92
eGFR (ml/min/1.73m ²)	95	116	79
Urea (mmol/L)	5.1	3.9	6.9
Residual Bladder Volume (mL)	78	224	165
Post Radical Prostatectomy			
Primary Pattern	3	3	3
Secondary Pattern	4	4	4
Tertiary Pattern	5	none	none
Overall Gleason Score	7	7	7
Pathological T-Stage	pt3b	pt3a	pt2c
Pathological N-Stage	pn0	pno	pn0
Pathological P-Stage	pmx	pmx	pmx

Table 1: Clinically relevant information for three patients who completed the study, including pre-treatment procedures, screening bloodwork, and post radical prostatectomy procedures.

3.2.2 Sodium Imaging Exam Protocols

High-resolution T_2 -weighted (T_2 -w) cube images (TE: 162 ms, TR: 2000 ms, FOV: 140×140 mm, voxel size: $0.44 \times 0.73 \times 1.4$ mm, flip angle: 90°) were acquired using a standard inflatable ^1H endorectal (ER) coil to allow for registration to histopathology.

^{23}Na imaging was performed using a custom-built ER receive-only RF coil and dedicated asymmetric transmit-only birdcage RF coil described in Farag *et al.* (31). The ^{23}Na sequence was a broad-banded 3D efficient fast gradient recalled echo (bbefgre3D) with the following parameters, TE: 1.5 ms, TR: 80 ms, FOV: 140×140 mm, voxel size: $4.4 \times 4.4 \times 6$ mm, and flip angle: 85° . For registration purposes, a set of ^1H axial, T_2 -w images were acquired (TE: 139.2 ms, TR: 5300 ms, FOV: 140×140 mm, voxel size: $1.09 \times 1.09 \times 3$ mm, and flip angle of 90°); the ^1H axial T_2 -w images were taken with the ^{23}Na ER coil inserted to provide morphological context for the ^{23}Na images and to facilitate co-registration with a master set of 3D T_2 -w images. For each patient, topical anesthetic Xylocaine (2%) was applied before insertion of the ER coil. Three calibration vials containing 30, 90, and 150 mmol/L of NaCl within the ^{23}Na ER coil were used to scale the sodium signal to absolute concentrations according to Farag *et al.* (31).

3.2.3 Ex-Vivo Imaging Exam

The prostate specimens were immobilized in a syringe of Christo-Lube MCG 1046 (Lubrication Technology, Franklin Furnace, Ohio), which is an MR-invisible fluorinated lubricant that produces no MRI signal and also minimizes magnetic susceptibility artifacts at the tissue-prostate boundary. Excised prostates were prepared (described below) and imaged with both T_1 -weighted (T_1 -w) (TE: 2.34 ms, TR: 6.41, FOV: $140 \times$

140 mm, voxel size: $0.73 \times 0.55 \times 0.6$ mm, flip angle: 15°) and T_2 -w (TE: 114 ms, TR: 2000 ms, FOV: 140×140 mm, voxel size: $0.73 \times 0.44 \times 0.6$ mm, flip angle = 90°) imaging contrasts using a 6-channel ^1H carotid coil. These images assisted in accurate registration to histopathologic registration.

3.2.4 Whole-Mount Histopathology

Following radical prostatectomy specimens were marked with cotton threads soaked with a blue tissue dye doped with gadolinium. Three threads were pierced through the prostate, and seven threads were fixed to the surface to serve as fiducial markers, prior to *ex-vivo* MRI. The prostate midglands were sliced into ~ 4 -mm transverse sections before paraffin embedding, leaving enough of the apex and base to be sagittally sliced for routine pathology analysis. Using a microtome, a $4\text{-}\mu\text{m}$ slice was obtained from each section and stained with H&E. The slides were then scanned at high resolution ($0.5\text{-}\mu\text{m}$ isotropic resolution, 24-bit colour) using a bright-field slide scanner (ScanScope GL; Aperio Technologies, Vista, California) and subsequently contoured (Gleason Grading) and confirmed by a pathologist (32). Cathie Crukely, Dr. Mena Gaed and Dr. Jose Gomez-Lemus contributed to histopathology.

3.2.5 Registration

Co-registration of image data was necessary due to the deformation of tissue, caused by differing geometries of the ER probes and the uncompressed nature of the tissue *ex-vivo*. Comparison of contoured histopathology and ^{23}Na MRI data was achieved through a complex registration pipeline, involving several image contrasts. The registration pipeline is an important and unique part of this research study. **Figure 4** outlines all image

contrasts used and their position in the pipeline. All registration was completed using 3D Slicer (Surgical Planning Laboratory, Harvard Medical School, Boston, Massachusetts), with a non-rigid, interactive, thin-plate spline (TPS) extension by Gibson, E. (2014) (33). Approximately 40 fiducial points were identified in pairs between two imaging volumes that were to be co-registered. Fiducials were placed on physiologically relevant ROIs, as well as patient-unique ROIs such as benign hyperplasia nodules and cystic spaces. In each registration, a reference volume and an input volume was chosen; where the reference volume remained unchanged and the input volume deformed according to the fiducial points.

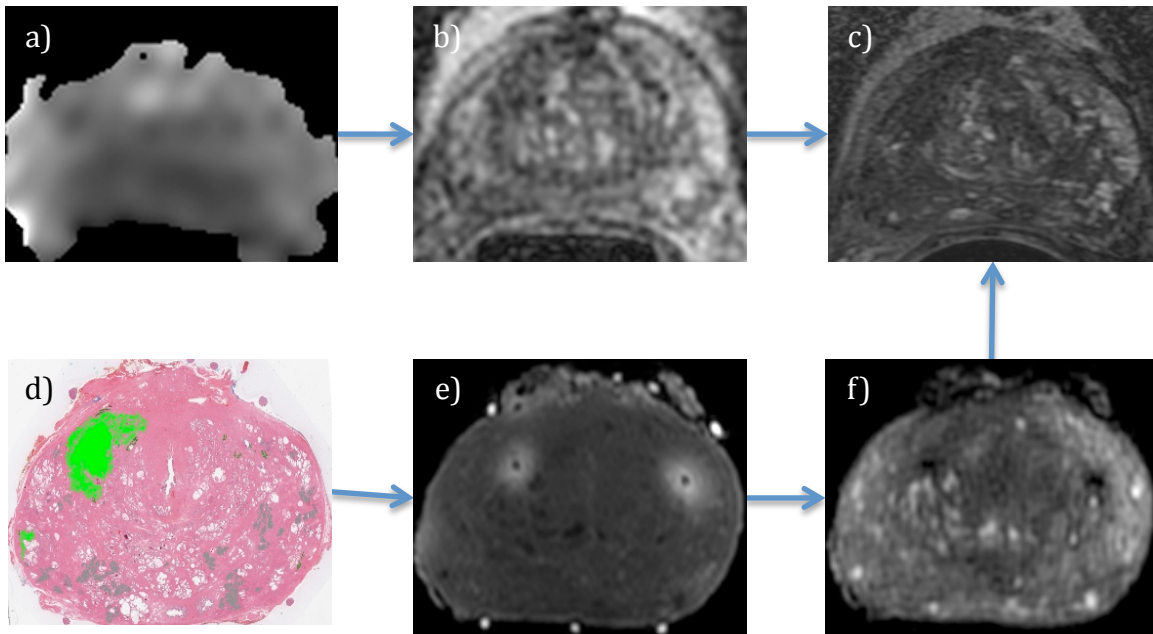


Figure 4: The registration pipeline for all imaging data involved in the study. The ^{23}Na volume, a) and body coil *in-vivo* T_2 -weighted volume, b) are registered to the endorectal *in-vivo* T_2 -weighted volume, c). The contoured histopathology, d) and the *ex-vivo* T_1 - and T_2 -weighted volumes (panels e) and f), respectively) are also registered to the endorectal *in-vivo* T_2 -weighted volume.

3.2.6 Statistical Analysis

Once each ^{23}Na MRI volume had been registered to corresponding histopathology, the pathologic contours on each slice were separated according to peripheral zone (PZ) and central/transitional zone (CTZ) as well as Gleason Score. In 3D Slicer, pathologic contours were imported as a separate mask from the remaining normal tissue and converted to scalar (gray scale) images. Each pathologic Gleason Score possessed its own unique intensity value, which were separated using a combined thresholding/ROI approach. This approach consisted of an initial manual selection of the bulk lesion, followed by an automated selection of the remaining pixels according to the desired pixel intensities. Within each histopathology image, Gleason Scores were separated into PZ and CTZ categories by manual segmentation on $T_2\text{-w}$ images. The anterior fibromuscular zone was not analyzed separately due to low ^{23}Na signal and an inability to distinguish the zone on mpMRI. The remaining tissue in the histopathology images was designated ‘normal tissue’ according to zone. The label maps were overlaid on the registered ^{23}Na images and the overlapping TSC values within the contours of the lesions were recorded. All data were imported into GraphPad Prism (v6.0f, GraphPad Software, San Diego, California) and subsequently analyzed using a one-way ANOVA (Tukey test) to assess significance between grades.

3.3 Results

Of the initial seven patients scanned with ^{23}Na MRI, 3 were included in the analyses. In the remaining four patients; two were scanned with an ER coil that did not include reference standards (TSC could not be calculated); one patient did not return for radical prostatectomy surgery so histopathologic information was not available; and data from the fourth patient was excluded due to uncorrectable motion during image acquisition. Clinically relevant patient information is provided in (Table 1). Six different Gleason Grade groups were observed (Figure 6), according to the primary and secondary features present.

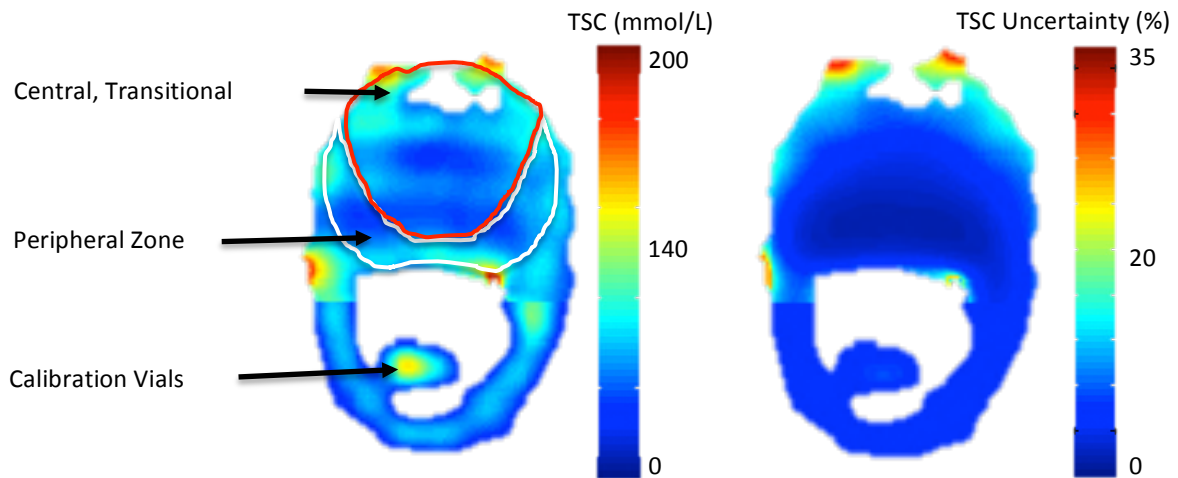


Figure 5: A representative, unregistered, coloured map of the tissue sodium concentration (TSC) in one slice with its corresponding measurement uncertainty in percentage. Central and transitional zones are combined, with the peripheral zone outlined separately.

Non-rigid registration of the ^{23}Na MR images to the contoured histopathology was accomplished to an accuracy of ~ 2 mm. The average TSC in normal peripheral zone tissue in all patients was measured to be 74.6 ± 6.7 mM (**Figure 5**). There was a statistically significant difference in TSC (**Figure 6**) between highly aggressive lesions (\geq Gleason 4+3) and moderately aggressive lesions (\leq Gleason 3+4) for Patients 1 and 2 ($p < 0.0001$); there were no Gleason 4+3 lesions present in Patient 3. The TSC between all Gleason Scores were significantly different ($p < 0.0005$), with the exception of PIN vs. Gleason 4+3 in Patient 1 ($p = 0.3776$), and PIN vs. Gleason 3 in Patient 2 ($p = 0.9892$).

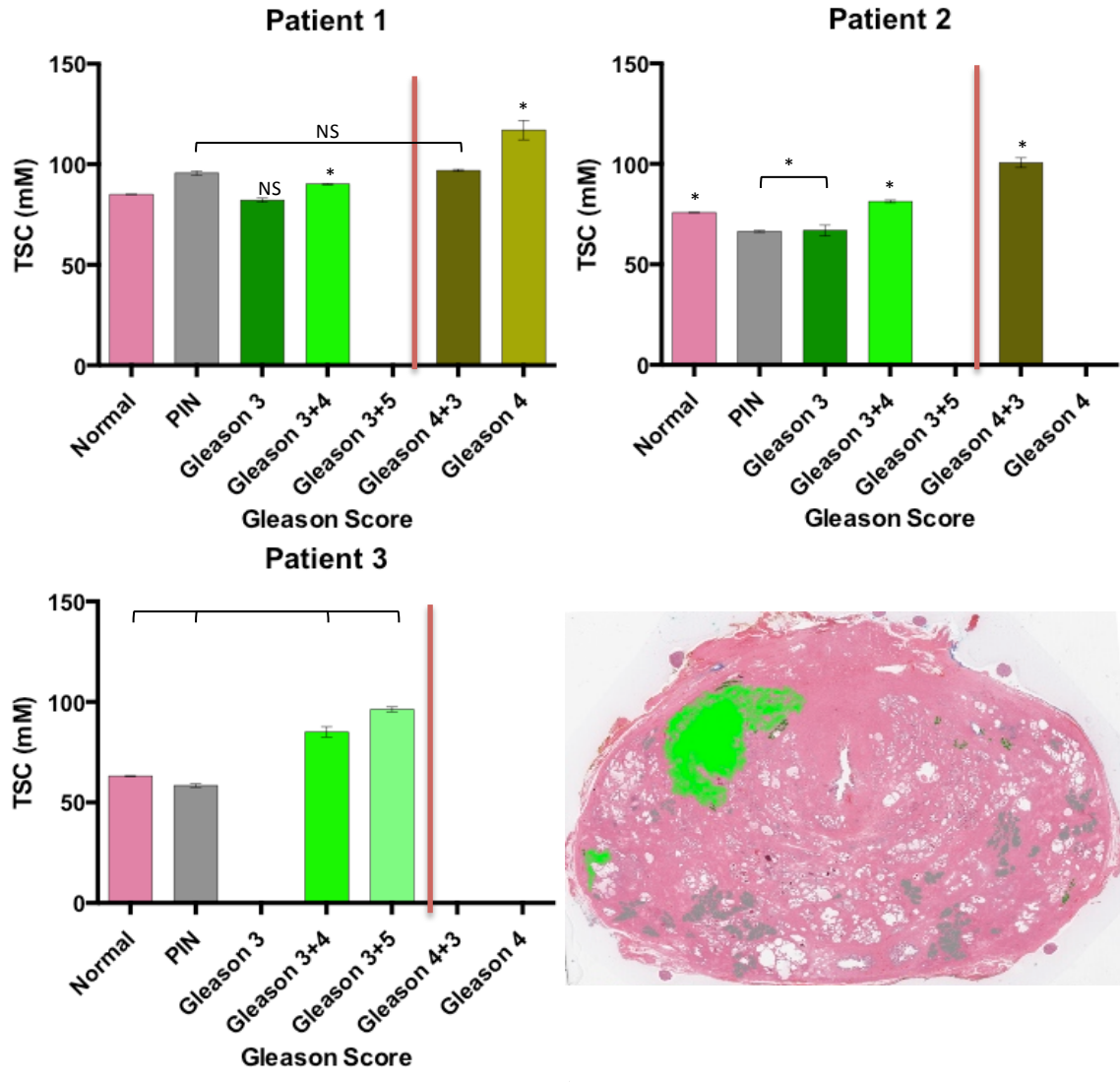


Figure 6: Three patients with biopsy proven prostate cancer underwent ^{23}Na MRI to determine the TSC in different grades of tumour tissue. The bottom right panel shows a representative histopathology slice from one patient. All Gleason Grade groups are significantly different from each other ($p < 0.05$) with the exception of PIN and Gleason 4+3 in Patient 1 and PIN and Gleason 3 in Patient 2. Red bars highlight the threshold between active surveillance and active treatment (Gleason 3+4/Gleason 4+3). Error bars represent one standard deviation for all voxels of that Gleason Score.

3.4 Discussion & Conclusion

We report the first *in-vivo* ^{23}Na MR measurements from a cancerous human prostate. TSC levels were significantly increased in lesions with a high Gleason Score when compared to a low Gleason Score, and that of normal tissue within respective zones. Previously, we have demonstrated that TSC can be consistently measured with high signal-to-noise ratio (SNR) over the entire prostate (31).

Dividing Gleason Score into qualitative low- (Gleason Score $\leq 3+4$), and high-risk (Gleason Score $\geq 4+3$) subgroups that correspond with treatment groups would establish the potential use for ^{23}Na MRI in prostate cancer diagnosis. Patients who fall into the low category should be monitored under the active surveillance branch in the National Comprehensive Cancer Network's (NCCN) guidelines (34). Patients in the high-risk category should undergo immediate treatment options within the NCCN's guidelines. While Cancer Care Ontario (CCO) maintains that patients with a Gleason Score of 7 should undergo active treatment, with the exception of select patients with low volume Gleason 3+4 PCa (8). More reliable noninvasive identification of biologically significant foci in the gland may enable targeted biopsy, focal therapy or focal dose escalation strategies (35–39).

This study involved the development and application of advanced MRI hardware and imaging data analysis including high-resolution whole-mount digital histopathology, and the ability to register it in 3D to MRI data to a high degree of accuracy (~ 2 mm). The histopathology alone required an average of 70 hours of time per prostate from an experienced pathologist. The registration pipeline incorporated a novel automated registration technique with sub-millimeter accuracy (40) as well as a manual, interactive

TPS technique (32), both capable of 3D, whole-volume registration. Accurate registration and detailed histopathology is essential in determining that the TSC measured in a specific ROI is in fact a cancerous lesion as determined by gold-standard histopathology (Figure 7). Finally, the development of sensitive integrated TORO RF hardware for sodium imaging was a key enabler for this research (31).

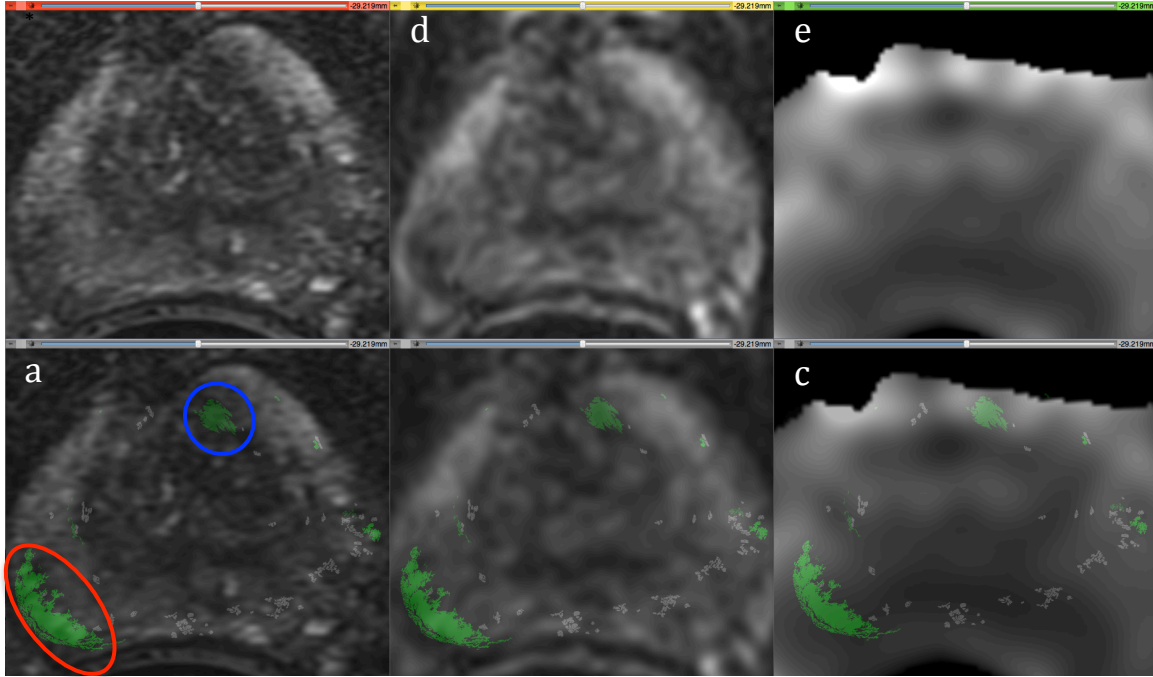


Figure 7: (a) high-resolution T₂-weighted ¹H Cube image, (b) an axially acquired ¹H T₂-weighted image, (c) and the distribution of endogenous sodium concentration (d-f) with corresponding histology contours overlaid of an oblique slice through a prostate with biopsy-proven cancer. Grey contours represent prostatic intraepithelial neoplasia (PIN, a possible precursor to cancer); blue and red outlines are Gleason 3 and Gleason 3+4 lesions, respectively.

The current study shows that TSC increases with increasing Gleason Score in patients with prostate cancer. While we are unable to associate this correlation with specific cellular changes, it is likely due to cellular reorganization (volume changes) and increased intracellular sodium concentration (24). With increasing Gleason Score, cellular density increases, which leads to a decreased extracellular volume. The

extracellular matrix, if in constant exchange with the vasculature, maintains a sodium concentration of ~140 mM (41), while the intracellular sodium concentration in normal prostate tissue is on the order of ~10-15 mM (18). Assuming a constant $[\text{Na}^+]_{\text{ex}}$, a cancerous IVF and EVF of 46.2% and 52.1%, respectively, and a normal IVF and EVF of 31.2% and 68.8%, respectively; $[\text{Na}^+]_{\text{in}}$ can be calculated for a given TSC value (42). The average TSC increase across all patients from normal tissue to Gleason 3+4 was ~11 mM (16%); therefore the $[\text{Na}^+]_{\text{in}}$ can be estimated to increase from 23.3 mM to 39.5 mM.

Cancer cells have been shown to exhibit an increased metabolism, which supplies the cell with enough energy to support accelerated proliferation and enhanced motility (43). The caveats of this increased metabolism include an upregulation of the sodium-proton (Na^+/H^+) antiport (25,26) and an inhibited sodium-potassium (Na^+/K^+ -ATPase) pump (17,27). As the tumor cell favors anaerobic glycolysis, the proton concentration within the cell increases reducing pH. Na^+/H^+ antiport is the major mechanism used to reduce the concentration of intracellular protons (16). As protons are pumped out decreasing the intracellular pH, the intracellular sodium concentration consequently increases. An acidic extracellular environment is also favored by the cancer cells, as it aids in cell motility (44) and invasiveness (45). The increased $[\text{Na}^+]_{\text{in}}$ is not directly distinguishable from $[\text{Na}^+]_{\text{ex}}$ but with assumptions of a constant $[\text{Na}^+]_{\text{ex}}$ (19); and intracellular and extracellular volume fractions from PCa tissue (42) it is possible to indirectly estimate $[\text{Na}^+]_{\text{in}}$ from TSC.

A limitation of the TSC measurement method is the inability to directly differentiate intracellular and extracellular sodium signal. As a result, we are unable to precisely measure the intracellular sodium concentration without knowing the relative compartment sizes within the tissue (assuming a known extracellular concentration). In principle, triple quantum filtering (TQF) could be used to discriminate signal from only the bound sodium ions but bound sodium is not exclusively found in the intracellular compartment (46,47). TQF techniques also have limited SNR and high sensitivity to B_0 - and B_1 -inhomogeneities making it a technically difficult prospect (48). One limitation of this study is the small sample size, which limits the ability to make predictions about the general population.

Due to the limited sodium concentration in tissue, the spatial resolution of sodium MRI is modest compared to proton imaging ($\sim 5 \text{ mm}^3$ vs. $\sim 0.5 \text{ mm}^3$). The pulse sequence used in this study was a `bbfgr3D` sequence that traversed k -space according to a Cartesian trajectory. 3D-Spiral pulse sequences, which are optimized for fast T_2 relaxation and efficient coverage of k -space, could prove promising in increasing SNR. Further development in this area could potentially increase spatial resolution and/or reduce acquisition times.

The inherent limitation of a surface ER coil is the receive profile, in which the signal requires sensitivity correction; due to the inhomogeneous receive profile. This issue is apparent not only in ^{23}Na MRI but present in all prostate MRI (including ^1H MR), where high-resolution imaging requires the use of an ER coil.

²³Na MRI is not specific to cancerous lesions, that is, regions of low signal intensity (or TSC) are not necessarily regions of normal tissue and regions of high signal intensity are not necessarily cancerous lesions. ²³Na MRI could prove to be a valuable addition to mpMRI to characterize lesions but at this point is not specific enough to detect lesion and lesion boundaries, which could explain the variation of TSC with increasing Gleason Score.

3.5 References

1. Statistics CCSAC on C ed. Canadian Cancer Statistics 2013. 2013.
2. Draisma G, Etzioni R, Tsodikov A, Mariotto A, Wever E, Gulati R, Feuer E, De Koning H. Lead time and overdiagnosis in prostate-specific antigen screening: Importance of methods and context. *J. Natl. Cancer Inst.* 2009;101:374–383. doi: 10.1093/jnci/djp001.
3. Etzioni R, Penson DF, Legler JM, di Tommaso D, Boer R, Gann PH, Feuer EJ. Overdiagnosis due to prostate-specific antigen screening: lessons from U.S. prostate cancer incidence trends. *J. Natl. Cancer Inst.* 2002;94:981–990. doi: 10.1093/jnci/94.13.981.
4. Heijnsdijk E a M, der Kinderen a, Wever EM, Draisma G, Roobol MJ, de Koning HJ. Overdetection, overtreatment and costs in prostate-specific antigen screening for prostate cancer. *Br. J. Cancer [Internet]* 2009;101:1833–1838. doi: 10.1038/sj.bjc.6605422.
5. Dragomir A, Cury FL, Aprikian AG. Active surveillance for low-risk prostate cancer compared with immediate treatment : a Canadian cost comparison. 2014;2:60–68. doi: 10.9778/cmajo.20130037.
6. Bjartell A. The 2005 International Society of Urological Pathology (ISUP) Consensus Conference on Gleason Grading of Prostatic Carcinoma. *Eur. Urol.* 2006;49:758–759. doi: 10.1097/01.pas.0000173646.99337.b1.
7. Gleason DF. Histologic grading of prostate cancer: A perspective. *Hum. Pathol.* 1992;23:273–279. doi: 10.1016/0046-8177(92)90108-F.
8. Morash C, Tey R, Agbassi C, Klotz L, McGowan T, Srigley J, Evans A. A Quality Initiative of the Program in Evidence-Based Care (PEBC), Cancer Care Ontario (CCO) Active Surveillance for the Management of Localized Prostate Cancer. 2014.
9. Sedelaar JPM, Vijverberg PLM, de Reijke TM, de la Rosette JJMCH, Kil PJM, Braeckman JG, Hendriks AJM. Transrectal Ultrasound in the Diagnosis of Prostate Cancer: State of the Art and Perspectives. *Eur. Urol. [Internet]* 2001;40:275–284.
10. Scattoni V, Zlotta A, Montironi R, Schulman C, Rigatti P, Montorsi F. Extended and saturation prostatic biopsy in the diagnosis and characterisation of prostate cancer: a critical analysis of the literature. *Eur. Urol.* 2007;52:1309–1322. doi: 10.1016/j.eururo.2007.08.006.
11. Djavan B, Ravery V, Zlotta A, Dobronski P, Dobrovits M, Fakhari M, Seitz C, Susani M, Borkowski A, Boccon-Gibod L, Schulman CC MM. Prospective evaluation of prostate cancer detected on biopsies 1, 2, 3 and 4: when should we stop? *J. Urol. [Internet]* 2001;166:1679–1683. doi: 10.1016/S0022-5347(05)65652-2.

12. Hambrock T, Somford D, Huisman H. Relationship between apparent diffusion coefficients at 3.0-T MR imaging and Gleason grade in peripheral zone prostate cancer. *2011;259:453–461.*
13. Hoeks CCM a, Barentsz JJO, Hambrock T, et al. Prostate cancer: multiparametric MR imaging for detection, localization, and staging. *Radiology [Internet] 2011;261:46–66. doi: 10.1148/radiol.11091822.*
14. Weidner AM, Michaely HJ, Lemke A, Breitingner L, Wenz F, Marx A, Schoenberg SO, Dinter DJ. Value of multiparametric prostate MRI of the peripheral zone. *Z. Med. Phys. [Internet] 2011;21:198–205. doi: 10.1016/j.zemedi.2010.12.004.*
15. Barentsz JO, Richenberg J, Clements R, Choyke P, Verma S, Villeirs G, Rouviere O, Logager V, Fütterer JJ. ESUR prostate MR guidelines 2012. *Eur. Radiol. [Internet] 2012;22:746–57. doi: 10.1007/s00330-011-2377-y.*
16. Demaurex N, Grinstein S. Na⁺/H⁺ antiport: modulation by ATP and role in cell volume regulation. *J. Exp. Biol. [Internet] 1994;196:389–404.*
17. Cameron I, Smith N, Pool T, Sparks R. Intracellular Concentration of Sodium and Other Elements as Related to Mitogenesis and Oncogenesis in Vivo. *Cancer Res. [Internet] 1980:1493–1500.*
18. Ouwerkerk R, Bleich K, Gillen J. Tissue Sodium Concentration in Human Brain Tumors as Measured with ²³Na MR Imaging. *Radiology [Internet] 2003;23:529–537.*
19. Thulborn KKR, Davis D, Adams H, Gindin T, Zhou J. Quantitative Tissue Sodium Concentration Mapping of the Growth of Focal Cerebral Tumors With Sodium Magnetic Resonance Imaging. *Magn. Reson. ... [Internet] 1999;359:351–359. doi: 10.1002/(SICI)1522-2594(199902)41:2<351::AID-MRM20>3.0.CO;2-H.*
20. Keenan MJ, Niedergerke R. Intracellular sodium concentration and resting sodium fluxes of the frog heart ventricle. *J. Physiol. 1967;188:235–260.*
21. Rose CR, Ransom BR. Regulation of intracellular sodium in cultured rat hippocampal neurones. *J. Physiol. 1997;499 (Pt 3:573–587.*
22. Rose CR, Ransom BR. Gap junctions equalize intracellular Na⁺ concentration in astrocytes. *Glia [Internet] 1997;20:299–307. doi: 10.1002/(SICI)1098-1136(199708)20:4<299::AID-GLIA3>3.0.CO;2-1.*
23. Fraser S, Diss J, Chioni A. Voltage-Gated Sodium Channel Expression and Potentiation of Human Breast Cancer Metastasis. *Clin. Cancer ... [Internet] 2005:5381–5389.*

24. Ouwerkerk R, Jacobs M a, Macura KJ, Wolff AC, Stearns V, Mezban SD, Khouri NF, Bluemke D a, Bottomley P a. Elevated tissue sodium concentration in malignant breast lesions detected with non-invasive ^{23}Na MRI. *Breast Cancer Res. Treat.* [Internet] 2007;106:151–60. doi: 10.1007/s10549-006-9485-4.
25. Reshkin SJ, Bellizzi a, Caldeira S, Albarani V, Malanchi I, Poignee M, Alunni-Fabbroni M, Casavola V, Tommasino M. Na^+/H^+ exchanger-dependent intracellular alkalinization is an early event in malignant transformation and plays an essential role in the development of subsequent transformation-associated phenotypes. *FASEB J.* 2000;14:2185–2197. doi: 10.1096/fj.00-0029com.
26. Rotin D, Steele-Norwood D, Grinstein S, Tannock I. Requirement of the Na^+/H^+ exchanger for tumor growth. *Cancer Res.* [Internet] 1989;49:205–11.
27. Kometiani P, Liu L, Askari A. Digitalis-Induced Signaling by Na^+/K^+ ATPase in Human Breast Cancer Cells. *Mol. Pharmacol.* [Internet] 2005;67:929–936. doi: 10.1124/mol.104.007302.of.
28. Near J, Bartha R. Quantitative sodium MRI of the mouse prostate. *Magn Reson Med* 2010;63:822–827. doi: 10.1002/mrm.22196.
29. Hausmann D, Konstandin S, Wetterling F, Haneder S, Nagel AM, Dinter DJ, Schonberg SO, Zollner FG, Schad LR. Apparent diffusion coefficient and sodium concentration measurements in human prostate tissue via hydrogen-1 and sodium-23 magnetic resonance imaging in a clinical setting at 3T. *Invest. Radiol.* 2012;47:677–682. doi: 10.1097/RLI.0b013e318267bc6f.
30. Bae KT, Kim J-H, Furlan A, Moon C, Park B, Zhao T. Proton and sodium MR imaging of in vivo human prostate using dual-tuned body and endorectal coils at 7T. In: Vol. 1. ; 2010. p. 5273.
31. Farag A, Peterson JC, Szekeres T, Bauman G, Chin J, Romagnoli C, Bartha R, Scholl TJ. Unshielded asymmetric transmit-only and endorectal receive-only radiofrequency coil for ^{23}Na MRI of the prostate at 3 tesla. *J. Magn. Reson. Imaging* [Internet] 2014:n/a–n/a. doi: 10.1002/jmri.24798.
32. Ward AD, Crukley C, McKenzie C a., et al. Prostate: Registration of Digital Histopathologic Images to in Vivo MR Images Acquired by Using Endorectal Receive Coil. *Radiology* 2012;263:856–864. doi: 10.1148/radiol.12102294.
33. Gibson E. 3D fusion of histology to multi-parametric MRI for prostate cancer imaging evaluation and lesion-targeted treatment planning. The University of Western Ontario; 2014.
34. National Comprehensive Cancer Network. NCCN Clinical Practice Guidelines in Oncology (NCCN Guideline®). Prostate cancer. Version 2.2014. 2014.

35. Kanthabalan a, Emberton M, Ahmed HU. Biopsy strategies for selecting patients for focal therapy for prostate cancer. *Curr. Opin. Urol.* [Internet] 2014;24:209–217. doi: 10.1097/MOU.0000000000000046.
36. Van Den Bos W, Muller BG, Ahmed H, et al. Focal therapy in prostate cancer: International multidisciplinary consensus on trial design. *Eur. Urol.* 2014;65:1078–1083. doi: 10.1016/j.eururo.2014.01.001.
37. Kasivisvanathan V, Emberton M, Ahmed HU. Focal therapy for prostate cancer: Rationale and treatment opportunities. *Clin. Oncol.* [Internet] 2013;25:461–473. doi: 10.1016/j.clon.2013.05.002.
38. Chalasani V, Williams AK, Chin J. Contemporary results of focal therapy for prostate cancer using cryotherapy. *Panminerva Med.* [Internet] 2010;52:217–222.
39. Bauman G, Haider M, Van Der Heide U a., Ménard C. Boosting imaging defined dominant prostatic tumors: A systematic review. *Radiother. Oncol.* [Internet] 2013;107:274–281. doi: 10.1016/j.radonc.2013.04.027.
40. Gibson E, Crukley C, Gaed M, Gómez J a., Moussa M, Chin JL, Bauman GS, Fenster A, Ward AD. Registration of prostate histology images to ex vivo MR images via strand-shaped fiducials. *J. Magn. Reson. Imaging* 2012;36:1402–1412. doi: 10.1002/jmri.23767.
41. Olson BR, Forman MR, Lanza E, McAdam P a., Beecher G, Kimzey LM, Campbell WS, Raymond EG, Brentzel SL, Güttsches-Ebeling B. Relation between Sodium Balance and Menstrual Cycle Symptoms in Normal Women. *Ann. Intern. Med.* 1996;125:564–567.
42. Langer DL, van der Kwast TH, Evans AJ, Plotkin A, Trachtenberg J, Wilson BC, Haider M a. Prostate tissue composition and MR measurements: investigating the relationships between ADC, T2, K(trans), v(e), and corresponding histologic features. *Radiology* 2010;255:485–494. doi: 10.1148/radiol.10091343.
43. Tannock IF, Rotin D. Acid pH in tumors and its potential for therapeutic exploitation. *Cancer Res.* 1989;49:4373–4384.
44. Goetze K, Walenta S, Ksiazkiewicz M, Kunz-Schughart L a., Mueller-Klieser W. Lactate enhances motility of tumor cells and inhibits monocyte migration and cytokine release. *Int. J. Oncol.* 2011;39:453–463. doi: 10.3892/ijo.2011.1055.
45. Kato Y, Ozawa S, Miyamoto C, Maehata Y, Suzuki A, Maeda T, Baba Y. Acidic extracellular microenvironment and cancer. *Cancer Cell Int.* [Internet] 2013;13:89. doi: 10.1186/1475-2867-13-89.

46. Jelicks LA, Gupta RK. On the extracellular contribution to multiple quantum filtered ^{23}Na NMR of perfused rat heart. *Magn. Reson. Med.* [Internet] 1993;29:130–133. doi: 10.1002/mrm.1910290124.
47. Knubovets T, Shinar H, Navon G. Quantification of the contribution of extracellular sodium to ^{23}Na multiple-quantum-filtered NMR spectra of suspensions of human red blood cells. *J. Magn. Reson.* 1998;131:92–96. doi: 10.1006/jmre.1997.1337.
48. Benkhedah N, Bachert P, Semmler W, Nagel AM. Three-dimensional biexponential weighted ^{23}Na imaging of the human brain with higher SNR and shorter acquisition time. *Magn. Reson. Med.* 2013;70:754–765. doi: 10.1002/mrm.24516.

Chapter 4

4 Discussion & Future Work

4.1 Discussion

4.1.1 Overview

Sodium MRI is a non-proton (x -nucleus) contrast-agent-free imaging technique deriving image contrast from the density of endogenous ^{23}Na ions in tissue. Using ^{23}Na MRI, it was possible to quantify tissue sodium concentration *in-vivo*, which has been shown to be an indicator of cellular metabolism and membrane integrity (1). Two custom-built RF coils; an asymmetric transmit birdcage coil, and an ER receive coil, allowed for acquisition of MR signal from the ^{23}Na nuclei. The TPS registration made it possible to compare gold-standard, whole-mount histopathology grading of PCa with the sodium contrast with a registration accuracy of a few millimetres. Using ^{23}Na MRI, the first in-man quantification of sodium levels in the cancerous prostate was reported here.

4.1.2 Clarification

All *in-vivo* sodium contrast derived in this study was from endogenous ^{23}Na nuclei. No introduction of sodium by oral or intravenous routes or any other contrast agent was required. As a result, the imaging period was not limited by agent wash-in/washout kinetics, nor was any approval required for contrast agent administration.

The data analysis was categorized into PZ and CTZ to account for the differences in biologic functions, genetics, and prognoses between zones (2–4). Due to these differences, generalizations cannot be made about the whole prostate, only within zones.

It should also be noted that T_2 -w contrast alone is non-specific to PCa in the PZ and can also result from other low-intensity lesions such as scarring, hyperplasia, and prostatitis (5). PCa mpMRI exams may benefit from a complementary contrast such as ^{23}Na MRI, which is specific to PCa.

4.1.3 Clinical Significance

At this juncture, we have been able to image, quantify and accurately co-register TSC with histopathological findings for three men with PCa. All three of these cases showed a significant positive trend of increased TSC with Gleason Score. This finding is in agreement with the literature of both brain and breast cancers, where there was an increase in observed TSC in malignant tissue when compared to normal contralateral tissue (6,7). As shown in **Figure 6**, normal PZ tissue had a lower TSC, when compared with the progressively aggressive scores of PIN, Gleason 3, Gleason 3+4, Gleason 3+5, Gleason 4+3, and Gleason 4. Of further importance, was the significance between lesions with Gleason Score 3+4 and Gleason Score 4+3 (**Figure 6**). According to the NCCN and CCO, this threshold is of critical value; any patient with a Score of 3+4 or less ($\leq 3+4$) should be placed in active surveillance, while patients with a Score of 4+3 or greater ($\geq 4+3$) should undergo immediate treatment (8,9).

A recent review of low-risk PCa in Canada concluded that the health care system could save as much as \$100 million annually by correctly stratifying PCa patients in appropriate treatment schemes (10). The savings were attributed to avoiding treatment in patients who died from causes other than PCa (treatment not required) and patients still receiving active surveillance. Not only would proper treatment planning alleviate the economic burden of overdiagnosis, the benefits are also apparent in the quality of life of

patients. Even taking into consideration the clinical discomfort of treatment as well as the psychological burden of active surveillance, a patient's quality-adjusted life expectancy (QALE) is higher in patients who undergo active surveillance (QALE = 11.07) when compared to brachytherapy (QALE = 10.57), intensity-modulated radiotherapy (QALE = 10.51), and radical prostatectomy (QALE = 10.23) (11).

A practical limitation of ^{23}Na MRI at this time is the requirement of a multinuclear MR scanner with the corresponding specialized hardware. While not every MRI system is capable of detecting nuclei other than protons, existing systems could be upgraded for this capability. Multinuclear MRI systems are also becoming more common in hospitals in recent years (12).

4.2 Future Work

4.2.1 Twisted Projection Imaging

Twisted Projection Imaging (TPI) has the benefit of reducing the number of excitations (NEX) needed for a complete 3D image, therefore reducing the overall scan time. When acquiring signal in the frequency domain (k -space) TPI uses a series of spiral gradient trajectories, programmed onto corresponding cones of differing angles that cover one hemisphere of k -space. This technique allows for more efficient sampling of the higher frequencies that are responsible for image detail, while preserving the lower spatial frequencies that are responsible for general shape and overall image contrast (13). TPI has been used successfully in assessment of stroke (14), cardiac tissue (15), and brain cancer (6). Implementing TPI imaging for ^{23}Na MRI could substantially increase SNR affording reduced imaging scan (~10 min.) and/or increased resolution for this contrast.

4.2.2 RF Hardware Improvements

The current study utilized an ER probe to receive sodium signal from the prostate and surrounding tissues, which led to the need for sensitivity correction of data for homogenous coverage over the prostate. The ER probe contains a single loop surface coil, resonating at the Larmor frequency of ^{23}Na nuclei at 3T. An inhomogeneous receive profile whose sensitivity drops off rapidly with distance from the coil loop is an inherent property of a surface coil. An external ^{23}Na tuned, non-rigid RF receive array coil, integrated with the existing transmit RF hardware would have the potential to produce a more homogeneous sodium contrast over the entire prostate. The array coil would be placed directly onto the pelvis of the patient to increase the penetration depth of imaging. Unfortunately, non-rigid array coils are subject to geometrical changes with patient anatomy and may require RF tuning on a per-patient basis, particularly due to the low gyromagnetic ratio of the ^{23}Na nucleus. Evaluation of the receive sensitivity for such an arrangement would also require further investigation.

The single-tuned nature of the ^{23}Na ER probe required the sequential insertion of two probes (^{23}Na and ^1H), which is uncomfortable for the patient, and a time-consuming intermediary step. The use of a dual-tuned $^{23}\text{Na}/^1\text{H}$ ER probe would shorten total exam time and improve the overall patient experience. As mentioned above (3.2), a dual-tuned ER probe was initially developed, which was resonant at both sodium (^{23}Na) and proton (^1H) frequencies but its sensitivity at the sodium frequency was inferior to a sodium-only ER RF coil. Therefore, the dual-tuned ER coil was not used for this preliminary study; however, in future work, the advantages of such a coil may out-weigh the SNR penalty when one considers its benefits for image registration and patient comfort.

4.2.3 Additional MRI Contrast Comparisons

This research has established that the integrated transmit-only, receive-only RF hardware developed by Farag *et al.* (16), is capable of accurately determining sodium levels in prostate cancer. More importantly, these measurements of TSC in prostate lesions have been directly compared with Gleason Score through a unique image registration pipeline. This pipeline can also be used to investigate the correlation of other mpMRI contrasts (T_2 -w, DCE, and ADC) with Gleason grading and compare it with these sodium results. Currently there are no comparisons of T_2 -w and ADC image contrasts with the gold standard of pathology. If ^{23}Na MRI provided a significant advantage over current mpMRI contrast mechanisms in grading PCa, its utility within the clinic could be highlighted. The ability to distinguish between patients who should be placed in active surveillance and those who require immediate treatment shows great potential but requires further investigation.

4.3 Conclusion

This study highlighted the efficacy of *in-vivo* sodium magnetic resonance imaging for human prostate cancer. This thesis expanded on the work of Farag *et al.* (16) utilizing a ^{23}Na -tuned TORO RF coil system to image the prostate and translated the pre-clinical research of Bartha *et al.* (17) to non-invasively assess tissue sodium concentration in human prostate cancer. The purpose of this thesis was to examine the potential for the use of ^{23}Na MRI in the clinic as a non-invasive tool to aid clinicians in PCa treatment stratification. The sodium RF hardware was used to acquire quantitative endogenous sodium information, which is an indirect measure of cellular metabolism and integrity. The sodium contrast was registered to gold-standard Gleason Scores determined from

whole-mount histology, following radical prostatectomy. Analysis of these imaging data revealed a significant increase in TSC with increasing Gleason Score, as well as a significant difference between Gleason Scores 3+4 and 4+3. This distinction is of great importance because it is the threshold for defining treatment in the clinic. Prostate cancers with scores $\leq 3+4$ are typically classified for active surveillance while scores $\geq 4+3$ are identified for immediate treatment. With further research, sodium MRI has the potential to become a complementary mpMRI contrast for non-invasive grading and active surveillance of this disease.

4.4 References

1. Murphy E, Eisner D a. Regulation of Intracellular and Mitochondrial Sodium in Health and Disease. *Circ. Res.* 2009;104:292–303. doi: 10.1161/CIRCRESAHA.108.189050.
2. Guo CC, Zuo G, Cao D, Troncso P, Czerniak BA. Prostate cancer of transition zone origin lacks TMPRSS2-ERG gene fusion. *Mod. Pathol.* 2009;22:866–871. doi: 10.1038/modpathol.2009.57.
3. Noguchi M, Stamey T a, Neal JE, Yemoto CE. An analysis of 148 consecutive transition zone cancers: clinical and histological characteristics. *J. Urol.* 2000;163:1751–1755. doi: 10.1097/00005392-200006000-00027.
4. Augustin H, Hammerer PG, Graefen M, Erbersdobler A, Blonski J, Palisaar J, Daghofer F, Huland H. Insignificant prostate cancer in radical prostatectomy specimen: Time trends and preoperative prediction. *Eur. Urol.* 2003;43:455–460. doi: 10.1016/S0302-2838(03)00139-8.
5. Turkbey B, Pinto PA, Mani H, et al. Prostate Cancer: Value of Multiparametric MR Imaging at 3 T for Detection—Histopathologic Correlation 1. *Radiology* [Internet] 2010;255:89–99. doi: 10.1148/radiol.09090475.
6. Ouwerkerk R, Bleich K, Gillen J. Tissue Sodium Concentration in Human Brain Tumors as Measured with ²³Na MR Imaging. *Radiology* [Internet] 2003;23:529–537.
7. Ouwerkerk R, Jacobs M a, Macura KJ, Wolff AC, Stearns V, Mezban SD, Khouri NF, Bluemke D a, Bottomley P a. Elevated tissue sodium concentration in malignant breast lesions detected with non-invasive ²³Na MRI. *Breast Cancer Res. Treat.* [Internet] 2007;106:151–60. doi: 10.1007/s10549-006-9485-4.
8. National Comprehensive Cancer Network. NCCN Clinical Practice Guidelines in Oncology (NCCN Guideline®). Prostate cancer. Version 2.2014. 2014.
9. Morash C, Tey R, Agbassi C, Klotz L, MCGowan T, Srigley J, Evans A. A Quality Initiative of the Program in Evidence-Based Care (PEBC), Cancer Care Ontario (CCO) Active Surveillance for the Management of Localized Prostate Cancer. 2014.
10. Dragomir A, Cury FL, Aprikian AG. Active surveillance for low-risk prostate cancer compared with immediate treatment : a Canadian cost comparison. 2014;2:60–68. doi: 10.9778/cmajo.20130037.

11. Hayes JH, Ollendorf D a, Pearson SD, Barry MJ, Kantoff PW, Stewart ST, Bhatnagar V, Sweeney CJ, Stahl JE, McMahon PM. Active surveillance compared with initial treatment for men with low-risk prostate cancer: a decision analysis. *JAMA* 2010;304:2373–2380. doi: 10.1001/jama.2010.1720.
12. Richards TL. Multinuclear Magnetic Resonance Spectroscopic Imaging . In: *Encyclopedia of Analytical Chemistry*. John Wiley & Sons, Ltd; 2006. doi: 10.1002/9780470027318.a0110.pub2.
13. Thulborn KKR, Davis D, Adams H, Gindin T, Zhou J. Quantitative Tissue Sodium Concentration Mapping of the Growth of Focal Cerebral Tumors With Sodium Magnetic Resonance Imaging. *Magn. Reson. ... [Internet]* 1999;359:351–359. doi: 10.1002/(SICI)1522-2594(199902)41:2<351::AID-MRM20>3.0.CO;2-H.
14. Thulborn KR, Davis D, Snyder J, Yonas H, Kassam A. Sodium MR Imaging of Acute and Subacute Stroke for Assessment of Tissue Viability. *Neuroimaging Clin. [Internet]* 2015;15:639–653. doi: 10.1016/j.nic.2005.08.003.
15. Ouwerkerk R, Weiss RG, Bottomley P a. Measuring human cardiac tissue sodium concentrations using surface coils, adiabatic excitation, and twisted projection imaging with minimal T2 losses. *J. Magn. Reson. Imaging* 2005;21:546–555. doi: 10.1002/jmri.20322.
16. Farag A, Peterson JC, Szekeres T, Bauman G, Chin J, Romagnoli C, Bartha R, Scholl TJ. Unshielded asymmetric transmit-only and endorectal receive-only radiofrequency coil for ²³Na MRI of the prostate at 3 tesla. *J. Magn. Reson. Imaging [Internet]* 2014;n/a–n/a. doi: 10.1002/jmri.24798.
17. Near J, Bartha R. Quantitative sodium MRI of the mouse prostate. *Magn Reson Med* 2010;63:822–827. doi: 10.1002/mrm.22196.
18. Gibson E, Crukley C, Gaed M, Gómez J a., Moussa M, Chin JL, Bauman GS, Fenster A, Ward AD. Registration of prostate histology images to ex vivo MR images via strand-shaped fiducials. *J. Magn. Reson. Imaging* 2012;36:1402–1412. doi: 10.1002/jmri.23767.

Appendix A – Supplementary Methods

Multiparametric Proton MRI Protocol

Patients were instructed to fast 12 hours prior to the exam, as well as drink 30 mL of milk of magnesia the night before. Upon arrival, patients were subjected to a screening exam to ensure all exclusion criteria had been followed. After screening, patients were escorted to the scanner bed, where all imaging took place. Calibration scans were acquired before introducing the ^1H endorectal probe to locate the prostate. Xylocaine (2%) was applied as a topical anaesthetic before the insertion of the probe. After the ^1H probe was introduced, two diffusion-weighted imaging (DWI) sequences were acquired with b -values of 100 and $800 \text{ s}\cdot\text{mm}^{-2}$ to calculate an apparent diffusion coefficient (ADC) map; followed by a T_2 -weighted (T_2 -w) Cube ‘Master’ sequence; and a dynamic contrast-enhanced (DCE) 3D sequence. Imaging parameters from the three sequences can be found in **Table 2.5.1**. Following the mpMRI exam the ^1H probe was removed and the patient was given a ten-minute break before the sodium examination.

Imaging Contrast Method	TE/TR (ms)	FOV (mm)	Voxel Size (mm)	Flip Angle	Bandwidth (KHz)
Apparent Diffusion Coefficient MRI	68.1/5600	140×140	1.1×0.55×3.6	90°	250
Dynamic Contrast-Enhanced MRI	1.54/3.1	100×140	0.78×1.1×3	12°	83.3
T_2 -Weighted MRI	162/2000	140×140	0.44×0.73×1.4	90°	31.2

Table A: Imaging parameters (TE/TR, FOV, Voxel Size, Flip Angle, and Bandwidth) of ADC, DCE and T_2 -w contrasts acquired in the mpMRI session.

Detailed Registration Steps

2.7.1 Step 1

The initial registration step in the pipeline (**Figure 3.2.5.1a-b**) involved a rigid registration between the ^{23}Na volume and the ^1H Axial T_2 -w volume, acquired serially. This registration step was necessary to correct for any motion that may have occurred between ^{23}Na and ^1H sequences. Fiducial points were fixed to the three reference calibration vials before a simple rotation/translation matrix was applied.

2.7.2 Step 2

The second step in the pipeline (**Figure 3.2.5.1b-c**) was the first non-rigid registration necessary due to the differing geometry between the ^{23}Na and ^1H endorectal probes. Fiducial points were identified in pairs on both the ^1H axial T_2 -w volume and the ^1H Master T_2 -w volume on ROIs, as described above.

2.7.3 Step 3

The third step in the pipeline (**Figure 3.2.5.1f-c**) utilized the non-rigid registration because of the deformation of tissue after radical prostatectomy. In this registration, the *ex-vivo* T_2 -w volume was the input image data that were deformed to the ^1H Master T_2 -w reference.

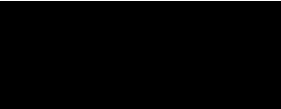
2.7.4 Step 4

The fourth step (**Figure 3.2.5.1e-f**) did not require any registration techniques because both volumes involved (*ex-vivo* T_1 -w and *ex-vivo* T_2 -w), were acquired in the same imaging session without movement of the sample.

2.7.5 Step 5

The fifth and final step (**Figure 3.2.5.1d-e**) registered the individual, digital whole mount histopathology images to the *ex-vivo* T_1 -w volume with sub-millimeter accuracy (18) by optimizing an affine transformation to minimize the fiducial registration error between the superficial and internal fiducial strands on MRI and the cross-sections of the fiducial strands on histology. Next, the TPS transformation was interactively defined to compensate for deformation between the *ex-vivo* and *in-vivo* MR images.

Appendix B – Hardware Approval



30 January 2013

Application No. 207004

Adam Farag, MSC




Re: Investigational Testing Application - Class II, Screening Acceptance Letter

Dear Adam Farag:

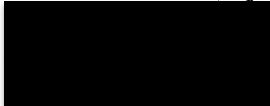
This is in reference to your Application for an Investigational Testing Authorization for the “Quadrature Asymmetric Bird Cage Radio Frequency Coil For Human Prostate and Whole Body Sodium 23 NA MR Imaging” received on 29 January 2013 and submitted pursuant to Part 3 of the *Medical Devices Regulations*.

We have accepted your application for processing towards an Investigational Testing Authorization.

This letter does not constitute a decision based on the review of submitted evidence in accordance with Part 3, Section 82(a) of the *Medical Devices Regulations*. The received information has been assessed only for the purpose of determining its acceptability for review.

If you have any questions regarding this request, please contact Dr. Fred Lapner, Section Head, Investigational Testing, at 

Yours sincerely,



Philip Neufeld, Ph.D.
Acting Manager
Device Evaluation Division
Medical Devices Bureau

PN/mw



Health
Canada

Santé
Canada

Health Products
and Food Branch

Direction générale des produits
de santé et des aliments

Therapeutic Products Directorate

DATE: FEB 21 2013

Application No. 207004

Adam Farag, MSc



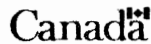
Investigational Testing Authorization - Class II

Dear Adam Farag:

This is in reference to your application for Authorization to conduct Investigational Testing in Canada, received on 29 January 2013 and submitted pursuant to Part 3 of the *Medical Devices Regulations*. This pertains to the following:

- Protocol:** Multi-modality Prostate cancer Image Guided Interventions
Type of diagnosis: prostate cancer
- Number:** Protocol #: IGPC-2
- Objectives:**
 - 1- To validate individualized hybrid imaging maps (HIM) based on a pre-operative imaging panel with actual cancer distribution in whole mount prostatectomy specimens.
 - 2- To compare the results of Sodium (²³Na) MRI with the PET/CT and the other MRI images collected in the study population undergoing radical prostatectomy to see if there may be additional information to determine the location and extent of cancer in the prostate.
- Device:** Quadrature Asymmetric Bird Cage Radio Frequency Coil for Human Prostate and whole body Sodium ²³Na MR Imaging
- No. of devices:** Two (2)
- No. of subjects:** Three hundred (300)

The information has been reviewed and you are hereby authorized under Section 83 of the *Medical Devices Regulations* to sell the subject device for investigational testing to the institution(s) listed in the attached Appendix 1.



F:\Mdb-bmm\3y Regulations\Part 3\Authorizations for Investigational Testing\Authorizations by Manufacturer's Name\Robarts Research Institute\207004-IT auth. let.doc

Sections 86, 87 and 88 of the *Medical Devices Regulations* impose additional requirements regarding the advertisement, record keeping and labelling of devices involved in investigational trials. Please advise the Bureau of any changes to the device, protocol or list of investigators. Any changes to the device or protocol that fall outside the scope of the risk assessment of this protocol will require a new application.

Yours sincerely,



Director
Medical Devices Bureau

RR/sw
Attach.

Appendix 1 - List of Investigator(s) and Institution(s)

Application No. 207004

Date: FEB 21 2013



Appendix C – Human Participant Approval

Ke issue
13/02/27



Research Ethics

Use of Human Participants - Ethics Approval Notice

Principal Investigator: Dr. Joseph Chin
 File Number: 101038
 Review Level: Delegated
 Approved Local Adult Participants: 60
 Approved Local Minor Participants: 0
 Protocol Title: Multi-modality Prostate Cancer Image Guided Interventions (REB #18135)
 Department & Institution: Schulich School of Medicine and Dentistry/Oncology, London Health Sciences Centre
 Sponsor: Canadian Institutes of Health Research

Ethics Approval Date: February 25, 2013 Expiry Date: September 30, 2014
 Documents Reviewed & Approved & Documents Received for Information:

Document Name	Comments	Version Date
Addition of Co-investigator	J. Torchia	
Revised Western University Protocol	Revised: exclusion criteria, objectives & methodology	
Revised Letter of Information & Consent		2013/01/08
Sub-Study Letter of Information & Consent	Optional Sodium MRI Imaging	2013/01/08
Amendment	#2 (V 1.4) - received for information only	2013/01/06

This is to notify you that The University of Western Ontario Research Ethics Board for Health Sciences Research Involving Human Subjects (HSREB) which is organized and operates according to the Tri-Council Policy Statement: Ethical Conduct of Research Involving Humans and the Health Canada/ICH Good Clinical Practice Practices: Consolidated Guidelines; and the applicable laws and regulations of Ontario has reviewed and granted approval to the above referenced revision(s) or amendment(s) on the approval date noted above. The membership of this REB also complies with the membership requirements for REB's as defined in Division 5 of the Food and Drug Regulations.

The ethics approval for this study shall remain valid until the expiry date noted above assuming timely and acceptable responses to the HSREB's periodic requests for surveillance and monitoring information. If you require an updated approval notice prior to that time you must request it using the University of Western Ontario Updated Approval Request Form.

Members of the HSREB who are named as investigators in research studies, or declare a conflict of interest, do not participate in discussion related to, nor vote on, such studies when they are presented to the HSREB.

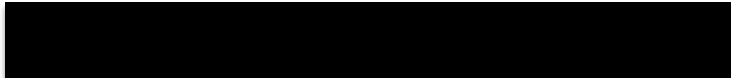
The Chair of the HSREB is Dr. Joseph Gilbert. The HSREB is registered with the U.S. Department of Health & Human Services under the IRB registration number IRB 00000940.



Ethics Officer to Contact for Further Information



This is an official document. Please retain the original in your files.



Appendix D – Data Collection Form

Protocol IGPC-2 Patient Initials: _____ Study #: IGPC2-0 _____

Multi-modality Prostate Cancer Image Guided Interventions **CASE REPORT FORM**

Patient's DOB: _____/_____/_____ (YYYY-MM-DD)

Cohort: Cohort 1 -Radical Prostatectomy Cohort 2 -Prostate Biopsy

Main Study Informed Consent

- Patient has read LOI
- Patient states understanding and all questions answered to their satisfaction
- Informed consent obtained, Date: _____/_____/_____
- Patient received copy of consent form

Optional PET/MRI Imaging Informed Consent

Did the patient agree to optional PET/MRI Imaging No Yes

If yes:

Date informed consent obtained: _____/_____/_____

Consent version date: _____/_____/_____

Optional Na MRI Imaging Informed Consent

Did the patient agree to optional Na MRI Imaging No Yes

If yes:

Date informed consent obtained: _____/_____/_____

Consent version date: _____/_____/_____

Protocol IGPC-2 Patient Initials: _____ Study #: IGPC2-0 _____

Multi-modality Prostate Cancer Image Guided Interventions
CASE REPORT FORM

Limited Medical History

	Yes	No*
Allergic reaction to Lidocaine gel (topical analgesic)		
Allergic reaction to Buscopan (anticholinergic/ system antispasmodic)		
Allergic reaction to Magnevist (contrast agent for MRI)		
Allergic reaction to iodine contrast (contrast agent for Dynamic CT)		
Allergic reaction to 18F-Choline (radio-isotope for PET scan)		
Contraindications to Buscopan such as myasthenia gravis, untreated narrow angle glaucoma, prostatic hypertrophy with urinary retention, stenotic lesions of the gastrointestinal tract, tachycardia, angina, cardiac failure or megacolon		
Contraindications to MRI such as pacemaker or other electronic implants, known metal in the orbit, cerebral aneurysm clips or claustrophobia.		

**All answers must be 'no' to maintain eligibility.*

Imaging Requisitions:

- PET/ CT Nuclear Medicine Requisition completed with patient**
- X-Ray Contrast Injection Patient Questionnaire**
- Robarts MRI Research Consent Form completed with patient**

**Please enter Robarts MRI Consent and X-ray Contrast Questionnaire into database.*

Patient instructed on MRI Prep:

- 30 mL of milk of magnesia night before
- NPO prior to exam by 12 hours

Patient instructed on PET/CT Prep:

- Clear fluids only and nothing to eat 4 hours prior
- 250 mL water 30 minutes prior to exam

Date Completed with patient: ____/____/____ (cannot be before consent date)

Protocol IGPC-2

Patient Initials: _____ Study #: IGPC2-0 _____

Multi-modality Prostate Cancer Image Guided Interventions
CASE REPORT FORM

Eligibility Criteria

Inclusion Criteria	Yes	No*
Provision of informed consent for this study.		
Male, aged 18 years or older.		
Pathologically confirmed prostate cancer on previous biopsy.		
Suitable for and consenting to radical prostatectomy for treatment of prostate cancer, or repeat biopsy as standard of care.		
Exclusion Criteria	Yes*	No
Prior therapy for prostate cancer (including hormone therapy), with the exception of radiation therapy for Cohort 2 only.		
Use of 5-alpha reductase inhibitors, i.e. finasteride (Proscar) or dutasteride (Avodart) within 6 months of study start. <i>Patients undergoing a 6-month washout period prior to study start will be eligible.</i>		
Inability to comply with the pre-operative imaging panel.		
Patients scheduled for radical prostatectomy with prostate size exceeding dimensions for whole mount pathology slides.		
Allergy to contrast agents to be used as part of the imaging panel.		
Sickle cell disease or other anemias.		
Insufficient renal function (eGFR <60 ml/min/1.73m ²).		
Residual bladder volume >150 cc (determined by post-void ultrasound).		
Hip prosthesis, vascular grafting or sources of artifact within the pelvis.		
Contraindication to MRI: <ul style="list-style-type: none"> o Pacemaker or other electronic implants o Known metal in the orbit o Cerebral aneurysm clips 		

*If any checkmarks appear in this column patient is ineligible.

Is patient eligible to continue? Yes No

Date of Eligibility Assessment: ____/____/____

Protocol IGPC-2 Patient Initials: _____ Study #: IGPC2-0 _____

Multi-modality Prostate Cancer Image Guided Interventions
CASE REPORT FORM

Pre-Treatment Procedures

Physical Exam including DRE Date: ____/____/____

Pre-biopsy PSA _____ ng/mL Date: ____/____/____

Date of Diagnostic TRUS Biopsy Date: ____/____/____ (confirming prostate cancer)

Prostate Volume (from TRUS Biopsy): _____ cc

Clinical Staging: cT1a cT1b cT1c cT2a cT2b cT2c

Pathological Staging: pT2a pT2b pT2c

Screening Bloodwork

Date of Tests: Date: ____/____/____

Were all tests performed on the same day? Yes No

Creatinine _____ $\mu\text{mol/L}$

eGFR _____ ml/min/1.73m² (must be ≥ 60)

Urea _____ mmol/L

Sickle Cell Screen Positive Negative

Date Post-Void Ultrasound Performed: ____/____/____

Residual Bladder Volume: _____ mL (must be <150 cc)

Protocol IGPC-2 Patient Initials: _____ Study #: IGPC2-0 _____

Multi-modality Prostate Cancer Image Guided Interventions
CASE REPORT FORM

Pre-Operative Imaging Panel

		Date of Scans YYYY-MM-DD
Imaging Day 1	Dynamic CT/ ¹⁸ F-FCH PET	____/____/____
	Optional PET/MRI or <input type="checkbox"/> N/A	____/____/____
Imaging Day 2	MRI (T1, T2, DWI, DCE, MRS)	____/____/____
	3D TRUS	____/____/____
	Optional Na MRI or <input type="checkbox"/> N/A	____/____/____

Was entire imaging panel completed? Yes No
If No, state reason: _____

Has all imaging been completed within a 2 week period? Yes No
If No, state reason: _____

Has all imaging been completed within 6 weeks of RRP/ Biopsy? Yes No
If No, state reason: _____

PROCEDURE

Cohort 1: Radical Prostatectomy

Date ____/____/____ Time: _____ Location: _____ Surgeon: _____

Type of Surgery: Open Robotic Assisted Laparoscopic

Please check all that are applicable:

- Nerve Sparing If yes, specify Unilateral R or L or Bilateral
- Non-nerve Sparing
- Sural nerve graft

Pelvic lymph node dissection performed?

- Yes
- No

Cohort 2: Prostate Biopsy

Date ____/____/____ Time: _____ Location: _____ Radiologist: _____

Protocol IGPC-2 Patient Initials: _____ Study #: IGPC2-0 ____

Multi-modality Prostate Cancer Image Guided Interventions
CASE REPORT FORM

18F-FCH PET/CT Scan

Date of ¹⁸F-FCH PET/CT Scan: ____/____/____

Time of ¹⁸F-FCH Injection: ____:____

Vital Sign Assessments Throughout ¹⁸F-FCH PET/CT Scan

	Time	Heart Rate (bpm)	Oxygen Saturation (%)	Blood Pressure (mmhg)
Baseline (prior to ¹⁸ F-FCH injection)				
Post PET Scan				

Were venous samples collected? Yes Not Done

If not done, reason: _____

Venous Sampling during ¹⁸F-FCH PET of Pelvis

Sample #	Sampling Time	Check if Obtained	If no, reason:
1- ¹⁸ FCH Injection	0 sec		
2	20 sec		
3	40 sec		
4	60 sec		
5	2 min		
6	3 min		
7	4 min		
8	6 min		
9	8 min		
10	12 min		
11	16 min		
12	20 min		
13	24 min		

Did any adverse events occur during PET/CT scanning? Yes No

If yes, record in AE log.

Protocol IGPC-2 Patient Initials: _____ Study #: IGPC2-0 ____

Multi-modality Prostate Cancer Image Guided Interventions
CASE REPORT FORM

Optional PET/MRI Scan

Consented to Optional PET/MRI? Yes No

If Yes, Date of Optional PET/MRI Scan: ____/____/____

Did any adverse events occur during PET/MRI scanning? Yes No
If yes, record in AE log.

Optional Na MRI Scan

Consented to Optional Na MRI? Yes No

If Yes, Date of Optional Na MRI Scan: ____/____/____

Did any adverse events occur during Na MRI scanning? Yes No
If yes, record in AE log.

MRI/MRS Scan

Date of MRI Scan: ____/____/____

Did any adverse events occur during MRI scanning? Yes No
If yes, record in AE log.

Was a 3D TRUS performed following the MRI? Yes No

If no, reason: _____

Protocol IGPC-2

Patient Initials: _____ Study #: IGPC2-0 _____

Multi-modality Prostate Cancer Image Guided Interventions
CASE REPORT FORM

Adverse Events

*AE reporting is restricted to the study period prior to Radical Prostatectomy or Biopsy (i.e. during imaging panel acquisition) as the Radical Prostatectomy and Biopsy are not considered part of the study intervention.

Were there any adverse events? No Yes, complete below.

Event	Start Date	Stop Date	Causality	Severity	SAE Y/N	Action Taken

Causality	Severity Grade	Action Taken
1 Unrelated	1 Mild	1 No action taken
2 Unlikely	2 Moderate	2 Medication taken
3 Possible	3 Severe	3 Imaging delayed/ stop prematurely
4 Probable	4 Life-threatening or disabling	4 Withdrawn from study
5 Definite	5 Death	88 Other- specify

CRF Completed By: _____ Date: _____

Appendix E – Curriculum Vitae

JUSTIN PETERSON

EDUCATION

- M.Sc. Medical Biophysics Candidate**, Western University 2013 - Present
- Specialization in Molecular Imaging
- B.Sc. (Hons) Medical Biophysics**, Western University 2008 - 2012
- Honours Specialization in Medical Biophysics (Physical Science Concentration)

AWARDS

- **Western Scholarship of Distinction:** 2008
 - Awarded to a student in 1st year with an average from 87-89.9%.

RESEARCH EXPERIENCE

- Undergraduate Honours Thesis (supervised by Dr. Blaine Chronik): “Investigating the effect of MR induced heating around passive medical implants in the sagittal plane.”
- Undergraduate Six-week Project (supervised by Dr. Blaine Chronik): “Radio Frequency Interactions with Medical Devices.”

VOLUNTEERING

- Security** – Palmer Rapids Twin Music Festival, Palmer Rapids, ON 2007 – Present
- Monitoring over 3000 patrons to ensure their safety and the success of the event
- Science Games Organizer** – Science Students’ Council, UWO 2009 – 2011
- Organized activities that provided a social outlet in order to increase community and pride within the faculty

PUBLICATIONS

- “Unshielded Asymmetric Transmit-Only and Endorectal Receive-Only Radiofrequency Coil for ²³Na MRI of the Prostate at 3 Tesla”, Farag A., **Peterson J. et al.**, J Magn Reson Imaging, (2014).
- “*In-Vivo* Sodium MRI of Prostate Cancer: Correlations with Gleason Grade Using Whole Mount Pathology”, **Peterson J. et al.**, Work in Progress.

CONFERENCE PROCEEDINGS

- “*In Vivo* Sodium Imaging of Human Prostate Cancer”, Poster Presenter, London Health Research Day, (2015).
- “*In Vivo* Sodium Imaging of Human Prostate Cancer”, Poster Presenter, Oncology Research and Education Day, (2015).

- “*In Vivo* Sodium Imaging of Human Prostate Cancer”, Poster Presenter, Proceedings of the ISMRM 23rd Scientific Meeting, (2015).
- “*In Vivo* Sodium MRI of Human Prostate Cancer”, Oral & Poster Presenter, 13th Annual Imaging Network Ontario Symposium, (2015).
- “Sodium MRI of *In Vivo* Human Prostate Cancer”, Poster Presenter, Scientific Meeting of the Ontario Institute for Cancer Research, (2015).
- “*In Vivo* Sodium MRI of Human Prostate Cancer”, Oral Presenter, Robarts Research Day, (2014).
- “²³Na MRI Applications in Human Prostate Cancer”, Second Place Poster Presenter, Cell Tracking Symposium, (2014).
- “*In Vivo* Sodium MRI of Human Prostate Cancer”, Poster Presenter, 12th Annual Imaging Network Ontario Symposium, (2014).
- “*In Vivo* Sodium MRI of Human Prostate Cancer”, Poster Presenter, Imaging Applications in Prostate Cancer, (2014).
- “*In Vivo* Sodium MRI of Human Prostate Cancer”, Poster Presenter, Windsor Cancer Research Group: International Cancer Research Conference, (2014).